Potassium in the Galactic Bulge – as traced by microlensed dwarf & sub-giant stars

Lukas Jönsson

Division of Astrophysics
Department of Physics
Lund University

2023-EXA203

Degree project of 15 higher education credits
June 2023

Supervisor: Thomas Bensby

Division of Astrophysics
Department of Physics
Box 43
SE-221 00 Lund
Sweden

Abstract

During this report the potassium (K) trend in the Galactic Bulge, with respect to metallicity and various α-elements, has been computed and evaluated by a method of line synthesis on the 7698.96 Å KI line (7699 KI), where Non-Local-Thermal-Equilibrium (NLTE) effects have been considered. Specifically, the α-elements of interest are calcium (Ca), titanium (Ti), silicon (Si), magnesium (Mg) and oxygen (O), due to the fact that these are believed to be valid tracer elements of Potassium due to their limited and/or well defined nucleosynthetic processes. The stellar sample used during the analysis is unique in the sense that it is the first sample of low- to intermediate- mass stars from the Galactic Bulge, making it possible to investigate age dependencies of the metallicity trends.

It is found that, for mildly metal-poor to metal-rich stars, almost all metallicity trends in the bulge exhibit large dispersion compared to what is found in disk(s). It is thus deemed uncertain to evaluate any age dependence's for any of the trends, the only slight exception being [K/O], where the dispersion is not as large as in the other trends, and a slight age dependence of increasing [K/O] as a function of decreasing age is observed. An investigation of why this dispersion occurs was performed, where it was found that the large majority of the dispersion was due a group of stars exhibiting a unpredictable spectral feature - the 7699 KI was blended with an unknown line of varying strength. Possible explanations of these unknown lines are hypothesized to be due to Diffuse Interstellar Bands (DIBs) or interstellar KI, both of which would yield similar anomalies found in the spectra of said group of stars.

It is thus assumed that no firm conclusion about the dispersion of the K-trends observed in the bulge can be made, due to the unknown nature of the blended lines. However, it is deemed probable that these blended lines contribute to a overestimation of the K abundance, but further investigation of these spectral features is necessary before any firm conclusions can be made about the K-trend and/ or possible enrichment of K in the Galactic Bulge.

List of Figures

3.1 Illustration of the effect on the synthetic spectrum depending if a NLTE or LTE model atmosphere is used. The stellar parameters of MOA-2010-BLG-049S are T_{eff} = 5694 K, log$g$ = 4.1, ξ_{micro} = 1.02, ξ_{macro} = 1.13 & [Fe/H] = −0.4 dex. 10

3.2 Distribution of abundances found for the Sun after 50 iterations, while analysing the asteroid Pallas. The K abundance of the Sun was found to be A(K) = 5.09 ± 0.04 dex. 11

3.3 **Top left:** Normalizing the spectrum by diving the flux by the slope of a linear regression fitted through four continuum-points. **Top right:** Fitting the observed spectrum to the synthetic by applying any wavelength or flux corrections necessary. **Bottom left:** Representation of the search of optimal abundance, where the grey lines represent different synthetic spectra of varying K abundance. **Bottom right:** χ^2 of abundance search. 12

4.1 Bulge stars, color-mapped by the age, compared to K in the Bensby et al. (2014) disk sample (Bensby in. prep.), colored light-grey. 13

4.2 Illustration of where various groups of stars are located relative to each other. Stars colored light-grey represent disk-stars, while stars colored grey represent bulge stars not members of the highlighted category. The color-mapped, or highlighted, stars represent various groups of stars that exhibit some kind of discrepancies. The plots are ordered such that the top row highlight *blended lines*, second row highlight *bad fits* and the third highlight all *outliers*. 15

4.3 Histograms comparing distributions of specific stellar parameters of *outliers* compared to *non-outliers*. 16

4.4 Abundance analysis of the outliers with *blended lines*, ordered such that the OGLE-2013-BLG-1793S correlate with the highest [K/Fe] and OGLE-2013-BLG-0446S correlate with the lowest [K/Fe] in this category. 17

4.5 Abundance analysis of the outliers with *bad fits*, ordered such that the MOA-2012-BLG-202S correlate with the largest [K/Fe] and OGLE-2013-BLG-1768S correlate with the lowest [K/Fe] in this category. 18

4.6 Metallicity trends of various α-elements. Grey and/ or color-mappend stars represent the bulge, while light-grey stars represent the disk(s). Specifically, stars that are color-mapped are *outliers*, where triangles represent *bad fits* and crosses represent *blended lines*. The abundances of the α-elements were previously determined by line synthesis in Bensby et al. (2017) & Bensby et al. (2021). 19

4.7 **Left:** [K/α] trends. **Right:** [K/α] trend with highlighted *outliers*. Color-scheme and markers is the same as in figure 4.6. 20

4.8 Normalized telluric spectrum, colored black, compared to normalized stellar spectra of MOA-2009-BLG-493S (solid line), MOA-2011-BLG-174S (dash-dotted line) and OGLE-2014-BLG-0157S (dashed line). It is important to note that comparisons such as this is done before any wavelength-corrections have been applied. 21

4.9 Illustration of where the merging line is located relative to the 7699 KI line, of spectrum from the *blended lines* category. 22

4.10 Figure from Maier et al. (2011), depicting how the strength of the DIB increase as a function of reddening (where ESPaDOnS and HD 203827 exhibit the least and most reddening, respectively). The spectra are aligned on their most prominent spectral feature. 23

4.11 Figure from Strassmeier & Weber (2020), depicting three spectra from the Henry Draper catalog, where HD 1 exhibit absorption lines from interstellar cloud containing K, with a non-zero relative velocity to HD 1, hence another 7699 KI emerge. 23

A.1 Abundance analysis of the 7699 KI line. 32

A.2 Abundance analysis of the 7699 KI line. 33

A.3 Abundance analysis of the 7699 KI line. 34

A.4 Abundance analysis of the 7699 KI line. 35

A.5 Abundance analysis of the 7699 KI line. 36

A.6 Abundance analysis of the 7699 KI line. 37

A.7 Abundance analysis of the 7699 KI line. 38

A.8 Abundance analysis of the 7699 KI line. 39

A.9 Abundance analysis of the 7699 KI line. 40

A.10 Abundance analysis of the 7699 KI line. 41

A.11 Abundance analysis of the 7699 KI line. 42

A.12 Abundance analysis of the 7699 KI line. 43
A.13 Abundance analysis of the 7699 KI line. 44
A.14 Abundance analysis of the 7699 KI line. 45
A.15 Abundance analysis of the 7699 KI line. 46
A.16 Abundance analysis of the 7699 KI line. 47

List of Tables

2.1 Descriptions of Einstein's light-matter interaction coefficients, which describe transition probability between certain quantum energy states. Unit of the coefficients are per particle, per second, per sterradian. 6

3.1 Stellar and instrumental parameters used to produce synthetic spectra by pySME, where *instrumental* referring to features of the spectrograph(s) used to gather the observed spectra. 9

4.1 Description of categories used to grade the line synthesis of specific stars, used to investigate if there exist any correlation between the unexpected dispersion found in figure 4.1. 14

Populärvetenskaplig beskrivning

Sökandet av förståelsen kring hur jorden, solsystemet, galaxen och universum fungerar har under de senaste hundratals åren varit ständiga frågor som vi människor grubblat över. Frågor som vad materia är, vart det kommer ifrån och hur det ter sig var under en lång tid obesvarade frågor. Idag vet vi att många grundämnen skapas genom den fusion som sker inuti stjärnkroppar, och resterande grundämnen skapas när stjärnor exploderar i så kallade supernovor. Vetenskapligt kallas denna process nukleosyntes, vilket i sin helhet beskriver skapandet av grundämnen.

Om vi anser fysikens lagar som universiella betyder det att nukleosyntes sker genom samma processer i fjärran galaxer som i vår egen galax, Vintergatan. För att underlätta analyser av fjärran galaxer är det därför viktigt att vi först noggrant analyserar hur varje grundämne ter sig i vår egen galax. Vår galax består främst av två centrala strukturer - det galaktiska centret och de galaktiska skivorna. Det är känt sedan länge att dessa galaktiska strukturer består av olika typer av stjärnpopulationer, och det är just därför vi måste göra jämförelser mellan dessa strukturer för att undersöka ifall den nukleosyntetiska processen för specifika ämnen beter sig på liknande vis överallt eller inte. Detta ger oss en helhetsbild som vi sedan kan använda som en mall när vi analyserar fjärran galaxer.

I detta projekt ska ett specifikt ämne, kalium, analyseras i det galaktiska centret. Anledningarna varför just kalium ska analyseras är flertal. Dels är den nukleosyntetiska processen för kalium inte helt förstådd då den sker i platser i stjärnatmosfären som är i icke-lokal-termisk-jämnvikt, vilket försvårar spektralanalysen avsevärt. Och dels då stjärnorna som ska analyseras är det första urvalet någonsin av denna typ av stjärnpopulation från det galaktiska centret - vilket gör det väldigt intressant, och framförallt möjligt, att undersöka hur kalium ter sig i centret jämför med skivorna.

Undersökningar kring om produktionen av kalium är kopplat till andra grundämnen, till exempel syre eller magnesium, är också av stort intresse. Då dessa har väl definierade nuklosyntetiska processer, samt inte är påverkade av effekter kopplat till icke-lokal-termisk-jämnvikt. Detta implicerar att om det finns en koppling mellan produktionen av kalium och dessa grundämnen skulle det vara fördelaktigt att analysera halter av dessa ämnen, istället för kalium, när man vill bestämma halter av kalium i t.ex fjärran galaxer, av den enkla anledningen att det är smidigare.

Contents

1 Introduction **1**

2 Theory **4**

2.1 Abundance Ratio 4

2.2 NLTE effects on Potassium 4

2.2.1 Spectral Line Formation 5

3 Abundance Analysis **7**

3.1 Data Collection & Stellar Parameters 7

3.2 Line Synthesis 8

3.2.1 Atomic data 9

3.2.2 NLTE-corrections 9

3.3 Uncertainty Analysis 10

3.4 Solar Potassium Abundance 11

4 Potassium in the Galactic Bulge **13**

4.1 Large Dispersion 14

4.2 α-elements 18

4.2.1 Outliers? 19

4.3 Outliers 21

4.4 Age dependence 23

5 Discussion **25**

5.1 Sophisticated Search Algorithms 25

5.2 Potassium Enrichment 25

5.2.1 AGB Outflows and Stellar Winds 26

5.2.2 Other Polluters 26

5.3 Blended Lines revisited 26

6 Conclusion **28**

A Plots of stellar fits and Chi^2 **32**

B Derivations **48**

B.1 Abundance Ratios 48

B.2 Source Function 48

B.3 Heliocentric Correction 49

Chapter 1

Introduction

The nucleosynthetic evolution of the Galaxy, and even the Universe, is governed by the nucleosynthetic yields of stars. If we rewind time to the beginning of star formation, the interstellar medium (ISM) supposedly only consisted primordial hydrogen (H), and possibly helium (He) (Arcones & Thielemann 2023), hence the chemical composition of early stars is believed to be just that, hydrogen and helium. In the present day we observe that the chemical composition of stars is much more complex, hence we ask the question *where did all the elements come from?*

The answer to this question is *nucleosynthesis*, which often reefer to the fusion of new atomic nuclei inside the core and/ or shell of stars. At the end of, or during, its life the star deposits the new chemical composition into the ISM by various process such as stellar winds and/ or supernovae, where the latter is also the host of various nucleosynthetic processes. In short, a fraction of the gas from which the star form transforms into metal at every iteration of star formation, which enrich the ISM such that the next generation of stars will start off with a slightly higher metal content than previous generations.

A combination of high apparent magnitudes and technological limitations makes it hard to acquire high-resolution spectra of distant galaxies. Thus to be able to evaluate and predict the chemical evolution of any galaxy, by so called tracer-elements, we must first find accurate abundance trends in our own Galaxy. Hence sophisticated spectroscopic analysis is required, which is possible by utilizing state-of-the-art spectrographs, e.g UVES mounted on the ESO's VLT (Dekker et al. 2000), that survey the sky and gather spectra of both high resolution and signal-to-noise ratio (S/N). While the nucleosynthesis of many elements is already well understood (Karakas & Lattanzio 2014) some elements still exhibit discrepancies between theoretical models and observations (Iliadis et al. 2016), which is the case of potassium (K).

Our Galaxy, the Milky Way, is a spiral galaxy which consist of three major structures - the bulge, the disk and the halo (Ryden & Peterson 2020), all of which exhibit differences regarding stellar population and kinematics. It turns out that the disk is composed of two structures - the thin and thick disk. In the jargon of astronomers young and metal-rich stars are called Population I, which is the dominant population of the thin disk, while old

and metal-poor stars are called Population II, which is the dominant population of the thick disk. It is also theorized that Population III stars exist, which are extremely massive stars composed of primordial gas (Tominaga et al. 2007). The Galactic Bulge contain stars of both population I and II (Ryden & Peterson 2020), while the halo is mainly composed of population II stars.

Gathering high-resolution spectra of low- to intermediate-mass stars in the Galactic Bulge is hard due to the random nature of microlensing events, which are needed due to the low luminosity of these types of stars (Ryden & Peterson 2020). Hence many previous studies of K have focused on stars located in the Galactic Disk(s). Several papers have attempted to determine the trends of K, see Zhang et al. (2006), Andrievsky et al. (2010), Zhao et al. (2016), Reggiani et al. (2019) & Zasowski et al. (2019), and while all agree that a trend of decreasing K with increasing metallicity exist there is disagreements of what the rate of change of this trend truly is. Though, as suggested by Takeda (2020) the discrepancies regarding rate of change might be due to lack of data, as most previous studies only contain a few dozen stars at most. Thus, Takeda performed a comprehensive study which consisted of *"a large sample of 160 FGK dwarfs and 328 late-G /early-K giants (including 89 giants in the Kepler field)"*. The dwarfs and 239 giants were located within tens and/ or hundreds of parsecs of the Sun, respectively, and classified as being members of the solar neighbourhood. The distance to the Kepler giants were wildly distributed, ranging from 0.1 to 2 kpc from the Sun. See figure 1 in Takeda (2020) for plots of relative positions and stellar parameters.

Takeda found a trend corresponding to d[K/Fe]/d[Fe/H] ≈ -0.1 to -0.15 for FGK Dwarfs, while thick-disk stars tend to show larger deviations from this gradient. Distant Kepler Giants showed little to no trend in any direction, hinting at the notion that the production of K might be location dependent due to the distinctly different distributions of each population. The study also suggested that there is no overall age dependence as only a slight trend was observed for dwarfs and no trend for giants.

Comparisons between K and other elements have also been made, to investigate if the production of K is coupled with any other elements. Zhang et al. (2006) found that the ratio [K/Mg] was nearly constant as a function of [Fe/H] and thus suggesting that the production of K was coupled with the α-element magnesium (Mg). Norregaard, C (2018) also made comparisons with α-elements but extending the search to titanium (Ti) as well, which showed similar trends as [K/Mg] - again suggesting that there might be a coupling between the production of K and α-elements.

Hence, this report will extend the study of K-trends in our Galaxy by determining the K-abundance of 77 stars from the Galactic Bulge. The stellar sample is unique in the sense that it is the first sample of low- to intermediate-mass stars from the Galactic Bulge, making it possible to determine the age of individual stars. Due to the uniqueness of the sample, abundance ratios and age dependence's with respect to iron (Fe) and various α-elements will be evaluated in comparison to trends found in the Galactic Disk(s).

This will be done by applying a method of line synthesis on the 7698.96 Å KI resonance line (7699 KI), along with sophisticated statistical analysis akin to a Monte Carlo simulation to find necessary uncertainties. Extra care for Non-Local-Thermal-Equilibrium (NLTE)

effects will be considered during the entire analysis, as K is seemingly severely affected by such effects (Reggiani et al. 2019). The line synthesis will be computed through the program pySME (Wehrhahn et al. 2023) and compiled and/ or evaluated by complimentary python code produced by the author of this paper.

Chapter 2

Theory

2.1 Abundance Ratio

When astronomers talk about abundance ratios it is usually in reference to the Sun, as this is the most convenient point of reference we have. To construct such a ratio we must first introduce the elemental abundance A(X), which represent the logarithmic abundance, or relative particle number density N(X), of element X with respect to H. Due to convention it is normalized such that A(H) = 12, see equation 2.1

$$A(X) = \log[N(X)/N(H)] + 12 \tag{2.1}$$

Now we introduce the notation $[X_1/X_2]$, see equation 2.2, which represent the abundance ratio between element X_1 and X_2 relative to the Sun. In this report ratios such as [K/Fe] and [Fe/H] will be of main interest, but ratios of K and α-elements, for example oxygen (O), will also be of great interest. See appendix B for full derivation of all abundance ratios analysed during this paper.

$$[X_1/X_2] = A(X_1) - A(X_1)_\odot - [X_2/H] \tag{2.2}$$

According to Gray (2021) the abundance of any weak line can be found by measuring the equivalent width and knowing the line strength (gf-value), that is the abundance is proportional to the equivalent width. However, instead of measuring equivalent widths this report will determine the abundance of K by line synthesis, see chapter 3 for further information.

2.2 NLTE effects on Potassium

According to Reggiani et al. (2019) the process responsible for K being sensitive to NLTE effects is mainly due to inelastic e+K scattering, that is, collisional excitation occur, which results in overpopulation of the ground state along with the first two excited states (4s,

$4p^{1/2}$ & $4p^{3/2}$) and thus the spectral line grow. It was also found that H+K collisional excitation and photo-ionization showed non-negligible contributions, but is most likely more prominent while analysing giants.

It is also worth noting that even though 1D NLTE effects are considered the synthetic spectra does not always fit the observed spectra in a satisfactory manner. This, based on studies of other elements such as lithium (Lind et al. 2013), is believed to be due to un-accounted 3D effects - that is, the discrepancies are due to 3-dimensional motion of convection cells in the envelope of the star which can make spectral lines deeper and/ or broader. For further analysis see figure 11 in Reggiani et al. (2019) for and comparison of the synthetic 7699 KI line, based on 1D LTE, 1D NLTE and 3D NLTE model atmospheres.

2.2.1 Spectral Line Formation

All spectral lines are formed by the same process - photons interact with the medium it travels through, where it either gets absorbed by or attenuates the medium. The former process produce absorption lines and the later produce emission lines. In short, the emergent intensity (I_ν) of a star is frequency dependent (ν) and is given by equation 2.3

$$\frac{dI_\nu(s)}{d\tau_\nu(s)} = S_\nu(s) - I_\nu(s) = \frac{j_\nu(s)}{\alpha_\nu(s)} - I_\nu(s), \tag{2.3}$$

where s denotes the distance between the source and the detector (while neglecting interstellar extinction), the source function $S_\nu \equiv j_\nu/\alpha_\nu$, describing the ratio of emission (j_ν) and extinction (α_ν) at a specific frequency and τ_ν being the optical depth. In more detail, emission and extinction at a given frequency can be described by the probabilistic nature of atomic level population.

The Einstein coefficients, see table 2.1, describe transition probabilities between certain energy levels, and can thus used to describe level population (n_i) of any energy level i. In short, see appendix B for full derivation, the source function can be expressed by the Einstein coefficients and/ or relations, see equation 2.4. In the case of Local-Thermal-Equilibrium (LTE) level population of certain energy levels, or energy partitioning, is described by the Saha-Boltzmann distribution, see equation 2.5, which transform the source function to a Planck function (B_ν) (Rutten 2003).

$$S_\nu = \frac{n_u A_{ul}}{(n_l B_{lu} - n_u B_{ul})} = \frac{2h\nu^3}{c^2}\frac{1}{\frac{g_u n_l}{g_l n_u} - 1} \overset{!}{=} \frac{2h\nu^3}{c^2}\frac{1}{e^{(-\Delta E/k_b T)} - 1} = B_\nu \tag{2.4}$$

$$\frac{n_i}{n_j} = \frac{g_i}{g_j} e^{(-\Delta E_{ij}/k_b T)}; \qquad \frac{n_i}{N} = \frac{g_i e^{(-\Delta E_i/k_b T)}}{\Sigma_n g_n e^{(-\Delta E_n/k_b T)}} \tag{2.5}$$

Coefficient	Description
A_{ul}	Spontaneous emission from upper (u) to lower (l) level.
B_{ij}	Stimulated transition from level i to j.
C_{ij}	Collisional transition from level i to j.

Table 2.1: Descriptions of Einstein's light-matter interaction coefficients, which describe transition probability between certain quantum energy states. Unit of the coefficients are per particle, per second, per sterradian.

$$\frac{dn_i(\vec{r})}{dt} = \sum_{j\neq i}^{N} n_j(\vec{r})P_{ij}(\vec{r}) - n_i(\vec{r})\sum_{j\neq i}^{N} P_{ij}(\vec{r}) = 0, \tag{2.6}$$

$$P_{ij} = A_{ij} + B_{ij}\vec{J_\nu} + C_{ij}; \qquad \vec{J_\nu} \equiv \text{Mean intensity of radiation field.} \tag{2.7}$$

In the case of Non-Local Thermal Equilibrium (NLTE) the Saha-Boltzmann approximation fails, hence another statistical approach has to be considered. According to Bergemann & Nordlander (2014) the statistical equilibrium of level population does not change with time, see equation 2.6 & 2.7, which implies that energy partitioning is not dependent on local behaviour alone and/ or that the coupling between level population and radiation field is non-linear and non-local. One can extent the formalism of LTE to account for NLTE effects by defining departure coefficients (Rutten 2003), see equation 2.8. The source function can then be expressed by equation 2.9, which is computationally useful when NLTE effects are considered.

$$b_i = \frac{n_i^{NLTE}}{n_i^{LTE}} \tag{2.8}$$

$$S_\nu = \frac{2h\nu^3}{c^2}\frac{1}{\frac{b_l}{b_u}(e^{(-\Delta E/k_bT)} - 1)} \approx \frac{b_u}{b_l}B_\nu \tag{2.9}$$

Chapter 3

Abundance Analysis

3.1 Data Collection & Stellar Parameters

The stellar sample used in this report is located in the Galactic Bulge, about 8 kpc from the Sun, and have been gathered over a number of years. This was done as a part of Target-Of-Opportunity (ToO), a programme with ESO's Ultraviolet and Visual Echelle Spectrograph (UVES) mounted on the Very Large Telescope (VLT) (Dekker et al. 2000) in Cerro Paranal, to combat the unpredicatble nature of microlensing events. The Microlensing Observations in Astrophysics (MOA) and Optical Gravitational Lensing Experiment (OGLE) surveys were used to find microlensing events in the bulge. Hence UVES collected the bulk of the data, but complementary observations was also made by the MIKE spectrograph (Bernstein et al. 2003) on the 6.5-m Magellan Clay telescope on Las Campanas and the HIRES spectrograph (Vogt et al. 1994) on the Keck telescope on Hawaii.

The stellar sample consists in total of 77 microlensed events, all of which acquiring a high resolution of $R \gtrsim 42000$ and signal-to-noise ratio in the range $15 \lesssim \mathrm{S/N} \lesssim 200$. The majority of the stars are located within $\pm 5^\circ$ of galactic longitude and in the range -2° to -5° of galactic latitude, see Fig. 1 in Bensby et al. (2017) for plot of relative positions, along with Bensby et al. (2010), Bensby et al. (2011), Bensby et al. (2013) for further information about data collection and verification that the stars are in fact located in the Galactic Bulge and other consistency checks.

The stellar parameters used in the analysis of this paper was determined by Bensby et al. (2017). Where the effective temperature ($\mathrm{T_{eff}}$) was determined from excitation balance of abundances of Fe I lines, and checked for consistency by comparing the wings of Balmer Hα lines between synthetic and observed spectra. See Fig D.1 in Bensby et al. (2017), which are seemingly in very good agreement with each other. Surface gravities ($\log g$) was determined from ionisation balance between abundances from Fe I & Fe II lines and the microturbulence (ξ_{micro}) determined from requiring that the strength of Fe I lines are independent of abundances. According to Bensby et al. (2017) the typical uncertainty of these parameters are $\Delta \mathrm{T_{eff}} \approx 100$ K, $\Delta \log g \approx 0.1$ to 0.2 dex and $\Delta[\mathrm{Fe/H}] \approx 0.05$ to 0.15

dex.

3.2 Line Synthesis

Line synthesis is a method of producing synthetic spectrum, by a model atmosphere, and fitting it to an observed spectrum. When a good fit has been found the input parameters which produced the synthetic spectrum is considered a reasonable representation of reality. The model atmosphere is dependent on a series of stellar parameters, such as effective temperature (T_{eff}), surface gravity ($\log g$) and metallicity ([Fe/H]), to name a few. See table 3.1 for full list of stellar parameters used during the line synthesis of this analysis.

In more detail, the calculations of the 1D model atmosphere are based on the plane parallel Uppsala MARCS code by Gustafsson et al. (2008), and are computed by the program pySME (Wehrhahn et al. 2023) - a python extension of Spectroscopy Made Easy (Valenti & Piskunov 1996). Which, if fed a linelist, simulates the radiative transfer and thus produces a synthetic spectrum by interpolating the stellar parameters and atomic data with a grid of pre-calculated model atmospheres. See section 3.2.1 for more information about the atomic data. To account for NLTE effects, a complimentary grid of NLTE departure coefficients from Amarsi et al. (2020) was utilized. Similarly, the departure coefficients are dependent on the stellar parameters in the same fashion as the model atmospheres.

In short, the general method of the analysis was to initialize pySME with all the fixed parameters, such as the stellar and instrumental parameters, and then apply a iterative method to find the optimal K abundance. In more detail, all of the data had to be pre-processed before any kind of evaluation could be made. This was done by first normalizing the observed spectra and fitting it, by convolution, to a synthetic "dummy" spectra (where "dummy" refer to a synthetic spectra produced with Solar abundances) such that any possible wavelength and/or flux corrections could be found. Then, synthetic spectra of a range of K abundances were created and evaluated by χ^2 (essentially squaring the difference between the observed and synthetic spectra over a range of wavelengths, often ± 0.2 around the core of the 7699 KI line). The evaluation of χ^2 was then fitted with a function ψ and the abundance that minimize ψ and/ or χ^2 was determined as the final abundance of the star. See figure 3.3 for visual illustration of the entire line synthesis process.

Parameter Name	Description
T_{eff}	Effective temperature of star.
log g	Surface gravity.
[Fe/H]	Overall metallicity of star, relative to the Sun.
[A/H]	Previously determined abundance of element A, relative to the Sun.
ξ_{micro}	Micro turbulence.
ξ_{macro}	Macro turbulence.
ipres	Resolution of the instrument(s).
iptype	Broadening profile of the instrument(s).

Table 3.1: Stellar and instrumental parameters used to produce synthetic spectra by pySME, where *instrumental* referring to features of the spectrograph(s) used to gather the observed spectra.

3.2.1 Atomic data

The atomic data used during the line synthesis is structured/ compiled as a linelist, which is a document that contain all relevant data, such as gf-values, broadening/ damping parameters and corresponding wavelength/ energy of all probable atomic transitions for any element. The atomic data is usually limited in some sense, by some stellar parameters and a wavelength interval. Specifically, the linelist used during the analysis of this report was sourced from the Vienna Atomic Line Database (VALD) (Kupka et al. 2000), and limited by the wavelength interval 7690 Å to 7707 Å. The solar stellar parameters $T_{\text{eff}} = 5772$ K, $\log g = 4.4$ and $\xi_{\text{micro}} = \xi_{\text{macro}} = 1$ km/s (Gray 2021) was also used to account for broadening effects correlated with the stellar parameters. It is also crucial to note that the linelist was exported in a *Long format* to include all the necessary data to consider NLTE calculations in pySME.

3.2.2 NLTE-corrections

Several reports, such as Zhang et al. (2006) & Takeda (2020), have made attempts to measure $\Delta\text{A(K)} = [\text{K/Fe}]_{\text{NLTE}} - [\text{K/Fe}]_{\text{LTE}}$ to investigate which values of certain stellar parameters contribute to the deviations from LTE, that is, which qualities of stars produce atmospheres where NLTE effects are prominent. It is generally found that high temperatures and low pressures yield largest deviations from LTE, and no relation between [Fe/H] and ΔA(K) is found for [Fe/H] $\gtrsim -1.5$ (Zhang et al. 2006).

The stellar parameters of the stellar sample analysed in this report is of approximately solar values, that is neither temperatures or pressures are of extreme nature. Hence, measurements such as ΔA(K) are ignored in this study, partly due to the argument made above, but mostly due to the fact that K is seemingly always influenced by NLTE effects (Reggiani et al. 2019). It is thus considered meaningless to try to determine the abundance while assuming LTE, as synthetic lines tend to grow wider instead of deeper with increasing

abundance. See figure 3.1 for visual demonstration of why an LTE model atmosphere is a poor approximation for the KI 7699 line.

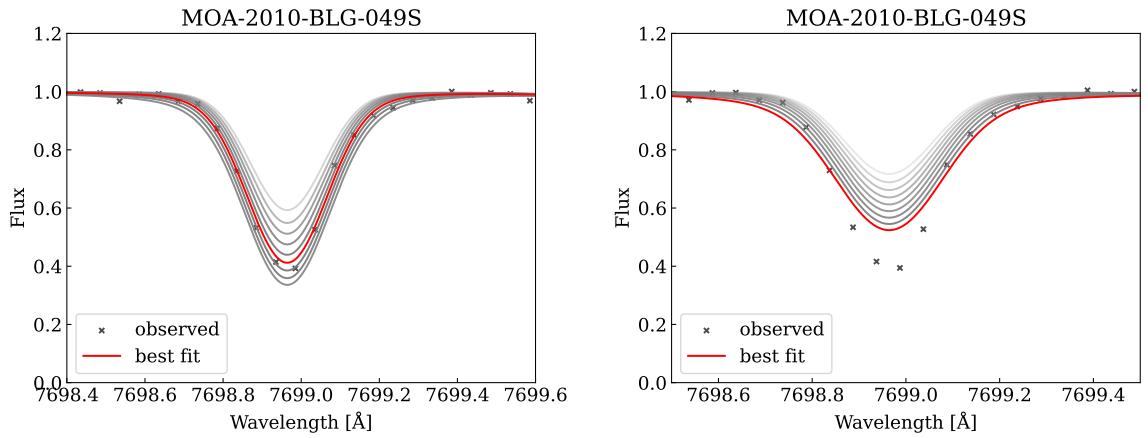

(a) Line synthesis where a NLTE atmosphere is being utilized.

(b) Line synthesis where a LTE atmosphere is being utilized.

Figure 3.1: Illustration of the effect on the synthetic spectrum depending if a NLTE or LTE model atmosphere is used. The stellar parameters of MOA-2010-BLG-049S are $T_{\rm eff} = 5694$ K, $\log g = 4.1$, $\xi_{\rm micro} = 1.02$, $\xi_{\rm macro} = 1.13$ & [Fe/H] $= -0.4$ dex.

3.3 Uncertainty Analysis

To combat statistical uncertainties an approach akin to a Monte Carlo simulation was employed, that is the uncertainty of all parameters used during the line synthesis were assumed to be members of distributions instead of a being discreet values, and that the uncertainties derived in Bensby et al. (2017) are standard deviations of each parameters distribution. For simplicity it was assumed that all distributions where Gaussian in shape.

For every spectrum an iterative method, where a random sample from every distribution of the parameters $T_{\rm eff}$, $\log g$, $\xi_{\rm micro}$, $\xi_{\rm macro}$ & [Fe/H], was used to re-synthesise the spectrum with a slightly different set of stellar parameters. This method, if repeated a number of times, yield a distribution of best abundances, see figure 3.2. This distribution is then used to find the most probable abundance along with margins of error, that is, the mean and standard deviation of the fitted Gaussian distribution, respectively.

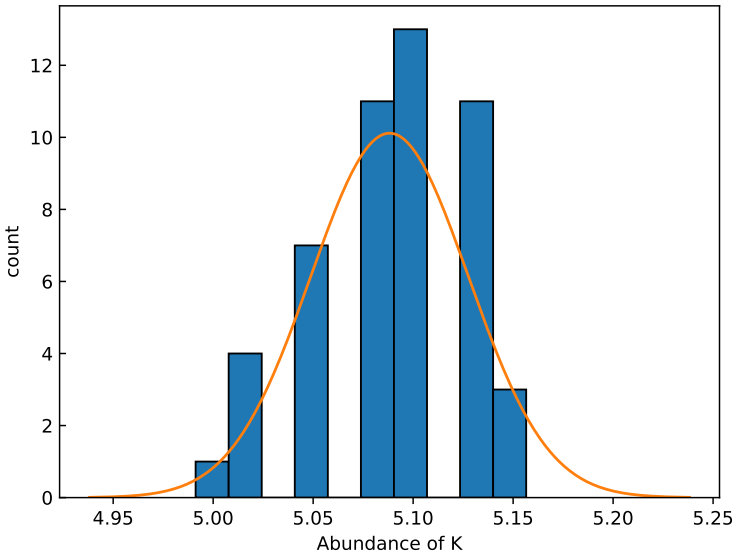

Figure 3.2: Distribution of abundances found for the Sun after 50 iterations, while analysing the asteroid Pallas. The K abundance of the Sun was found to be $A(K) = 5.09 \pm 0.04$ dex.

3.4 Solar Potassium Abundance

To avoid systematic uncertainties while determining the abundance ratio [K/Fe] the same method used on the stellar sample was employed on a solar spectrum. Specifically, the solar spectrum was gathered by UVES while observing the asteroid Pallas. The solar K abundance was found to be $A(K)_{\odot} = 5.09 \pm 0.04$, which is in great agreement with the value $A(K)_{\odot} = 5.08 \pm 0.07$ derived by Asplund et al. (2005), and is in good agreement, albeit being 0.03 dex lower, with $A(K)_{\odot} = 5.12 \pm 0.03$ derived by Zhang et al. (2006). See figure 3.3 for analysis of the 7699 KI resonance line in the Sun.

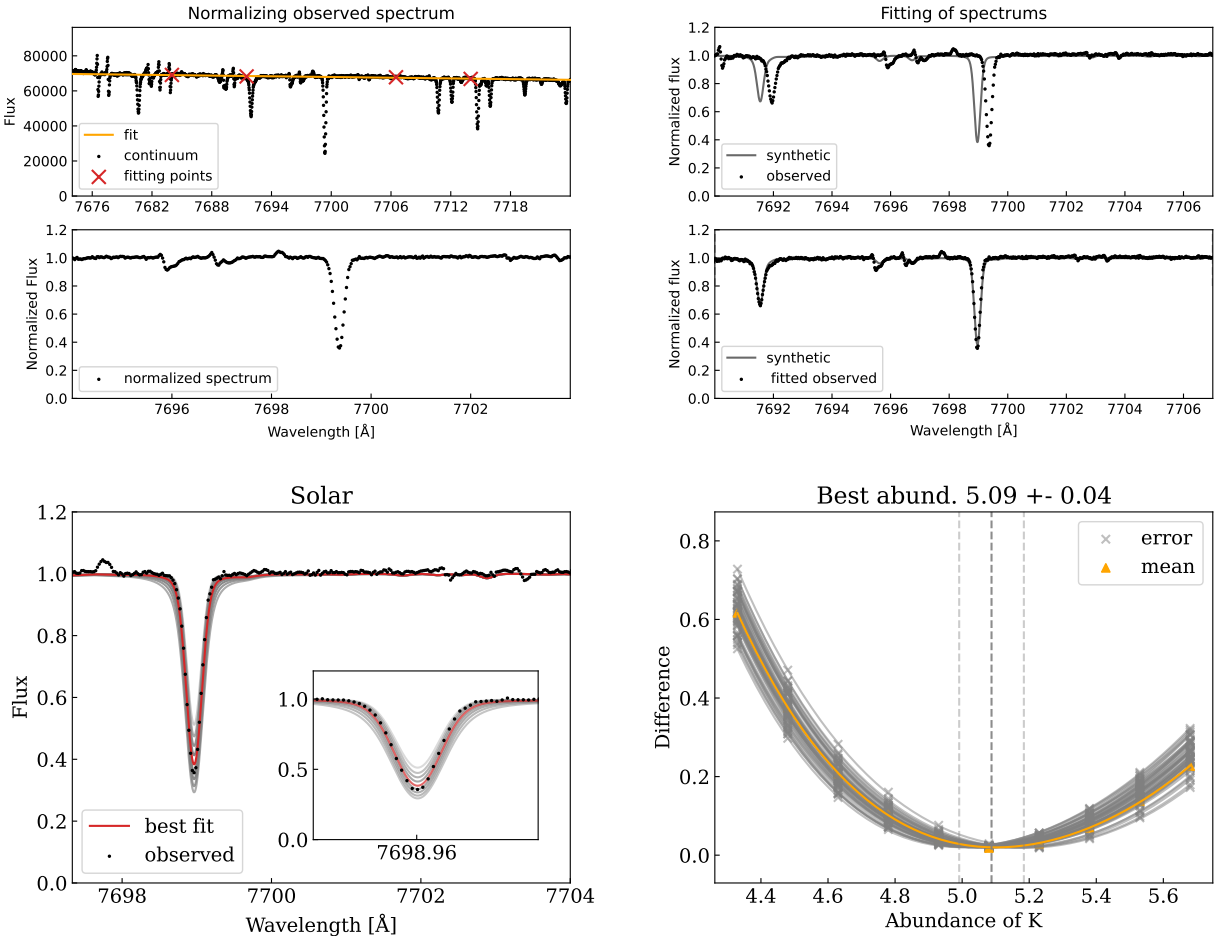

Figure 3.3: **Top left:** Normalizing the spectrum by diving the flux by the slope of a linear regression fitted through four continuum-points. **Top right:** Fitting the observed spectrum to the synthetic by applying any wavelength or flux corrections necessary. **Bottom left:** Representation of the search of optimal abundance, where the grey lines represent different synthetic spectra of varying K abundance. **Bottom right:** χ^2 of abundance search.

Chapter 4

Potassium in the Galactic Bulge

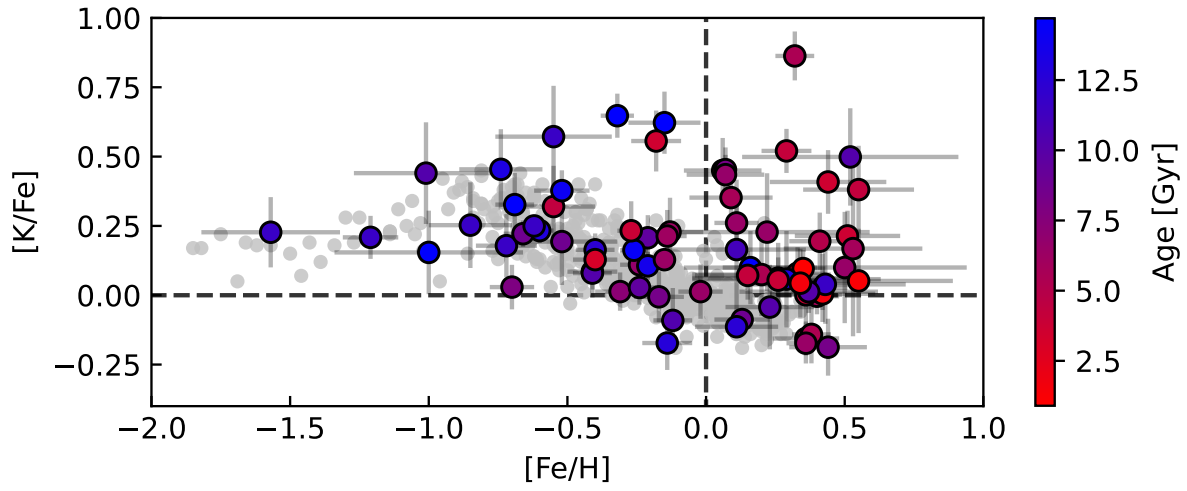

Figure 4.1: Bulge stars, color-mapped by the age, compared to K in the Bensby et al. (2014) disk sample (Bensby in. prep.), colored light-grey.

The compiled results of the abundance analysis is found in figure 4.1, where it is observed that for mildly metal-poor to metal-rich stars, i.e [Fe/H] $\gtrsim$ -0.5, there is a significant dispersion of the K abundance compared to the K abundance in the Bensby et al. (2014) disk sample (Bensby in. pro.), that is, a large portion of the bulge-stars seems to be significantly K enriched compared to stars in the disk(s). See section 4.1 & 5 for further investigation and discussion of why this dispersion may occur.

Abundance ratios between K and various α-elements have also analyzed, see figure 4.7 for ratios of K and calcium (Ca), silicon (Si), titanium (Ti), magnesium (Mg) and oxygen (O), where similar conclusions as above are made - the abundance of K in the bulge seems to be significantly larger than what is found in the disk(s), see section 4.2 for further discussion.

4.1 Large Dispersion

To investigate if the dispersion of the K-trend observed in figure 4.1 is a true occurrence or not the line synthesis of all spectra were visually graded according to two categories - *blended lines*, containing stars with a blended 7699 KI line, and *bad fits*, containing stars where the line synthesis was not satisfactory. The combination of the two categories are deemed *outliers*, due to their unique spectral features compared to the rest of the stellar sample, deemed *non-outliers*. See table 4.1 and figure 4.2(a) for specific description of the main categories along with visual representation of where these groups of stars located relative to each other, respectively.

Name	Description	Figure
Blended lines	Spectra containing a line within 0.5 Å of the 7699 KI line.	4.4
Bad fits	Spectra which the line synthesis was not satisfactory.	4.5
Outliers	Spectra of both *blended lines* and *bad fits*.	-

Table 4.1: Description of categories used to grade the line synthesis of specific stars, used to investigate if there exist any correlation between the unexpected dispersion found in figure 4.1.

From the bottom sub-figure in figure 4.2 it is observed that almost all stars contributing to the unexpected dispersion are *outliers*, where the majority belong to the *blended lines* category. By inspecting the line synthesis of all stars in the *blended lines* category, see figure 4.4, it is observed that the line synthesis is in fact not poor for the majority of the stars. The only clear exceptions being OGLE-2013-BLG-1793S and OGLE-2014-BLG-1122S, both of which severely overestimate the K abundance. Contrary, albeit expected, the opposite conclusion is made when investigating the stars in the *bad fits* category, see figure 4.5, where it is found that most of these synthetic spectra overestimate the K abundance.

Further investigation if these stars showcase any unique features was done by plotting histograms, comparing various stellar parameters of *outliers* and *non-outliers*, along with computing p-values by performing a 2-sided Kolmogorov-Smirnov test to see how statistically coupled two distributions are, see figure 4.3. It is found that all stellar parameters have p-values significantly greater than 0.05, with the slight exception of S/N which have a p-value of 0.16. This implies that the stellar parameters of *outlier*-stars do not belong to any unique population, that is, they are seemingly from the same population(s) as *non-outliers*. Hence the null hypothesis can not be rejected and no conclusion about what makes these stars special can be made, though it is worth noting that the p-value of the S/N parameter might indicate that the overall quality of the *outliers* is poor.

It is thus concluded that even if the dispersion due to the *bad fits* category can be explained by poor line synthesis this argument does not hold to explain the dispersion due to *blended lines*. And due to the different sizes of the two categories, the sample of *blended lines* being twice as large the sample of *bad fits*, it is suggested that the dispersion

of [K/Fe], or the general enrichment of K, observed in the bulge might be real - assuming the abundance analysis is correct. See section 4.3 for further analysis regarding the validity of the *outliers*.

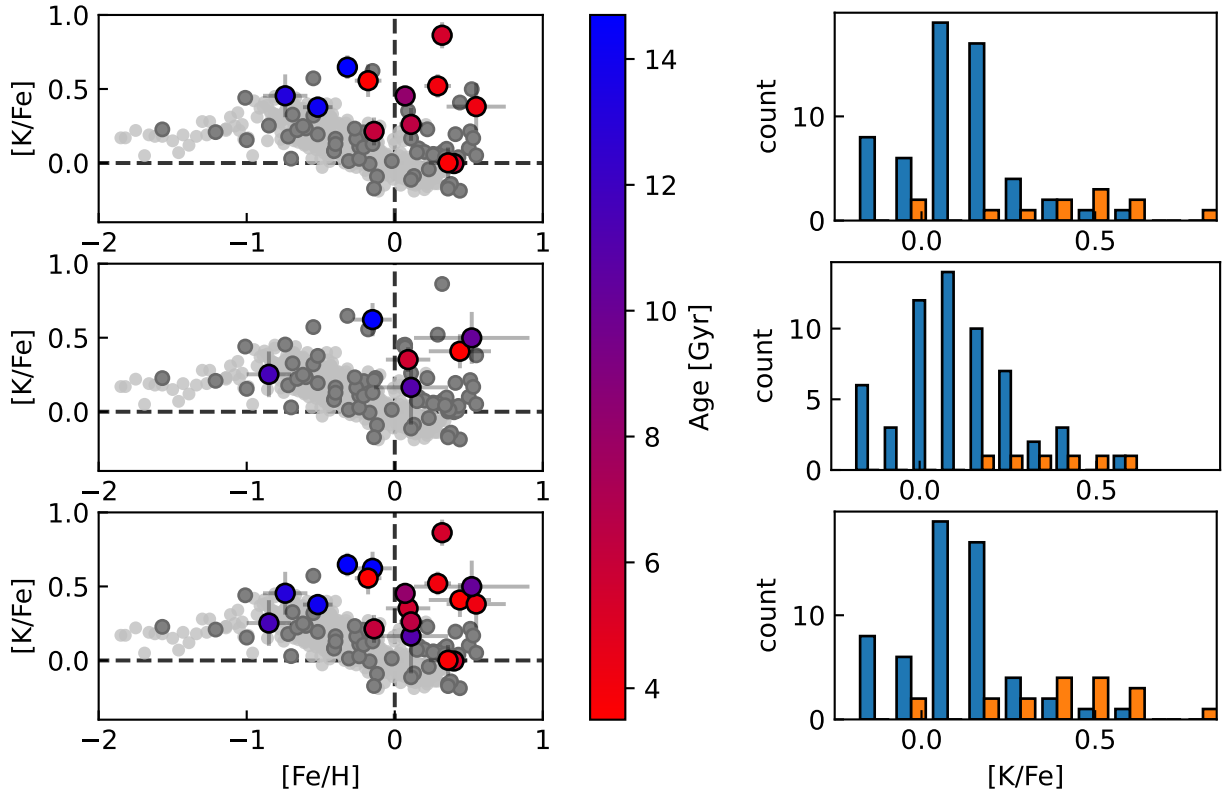

(a) To make the plot cleaner only highlighted stars have errorbars. See figure 4.1 errorbars of all stars.

(b) Blue are stars not members of the highlighted category.

Figure 4.2: Illustration of where various groups of stars are located relative to each other. Stars colored light-grey represent disk-stars, while stars colored grey represent bulge stars not members of the highlighted category. The color-mapped, or highlighted, stars represent various groups of stars that exhibit some kind of discrepancies. The plots are ordered such that the top row highlight *blended lines*, second row highlight *bad fits* and the third highlight all *outliers*.

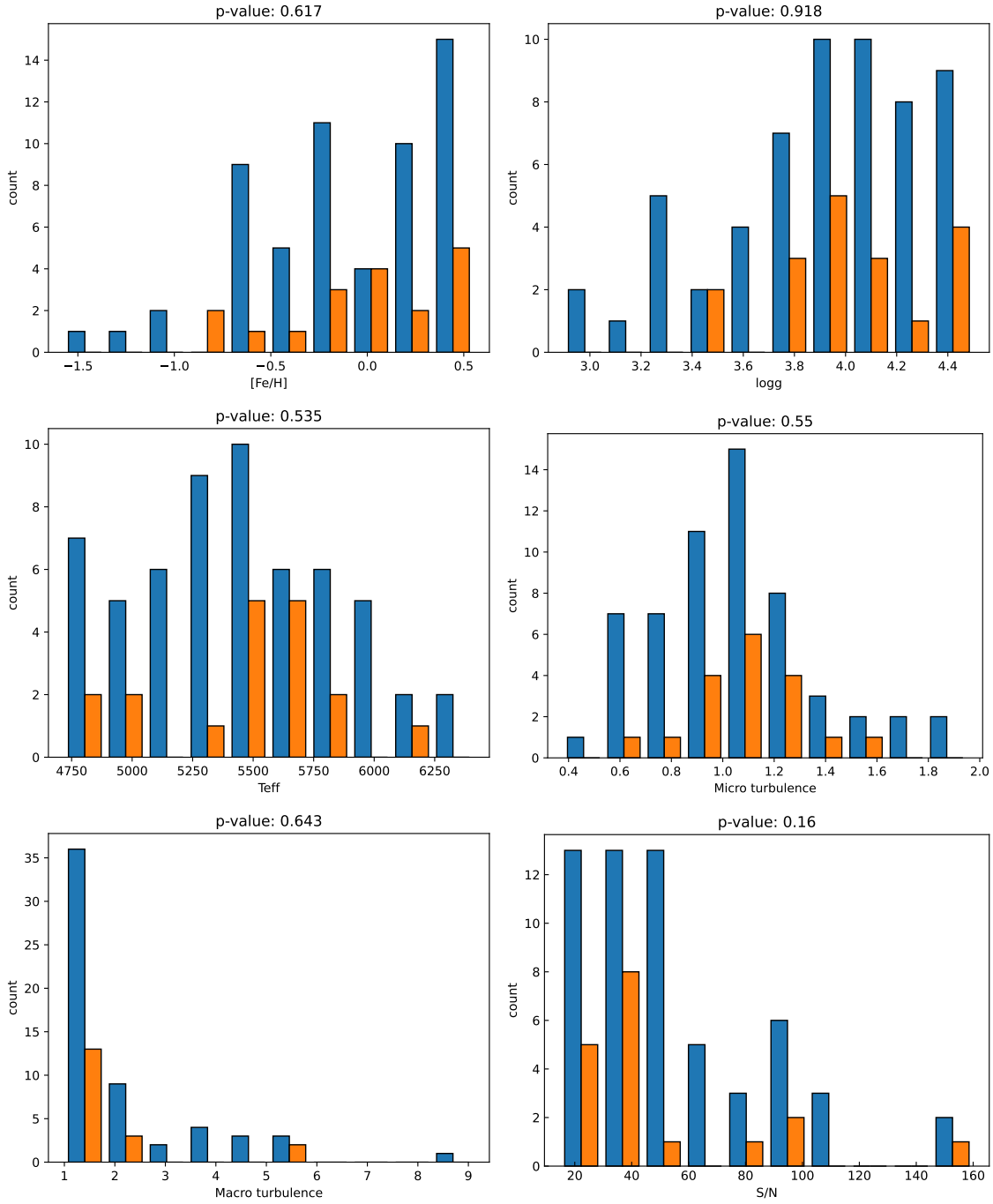

Figure 4.3: Histograms comparing distributions of specific stellar parameters of *outliers* compared to *non-outliers*.

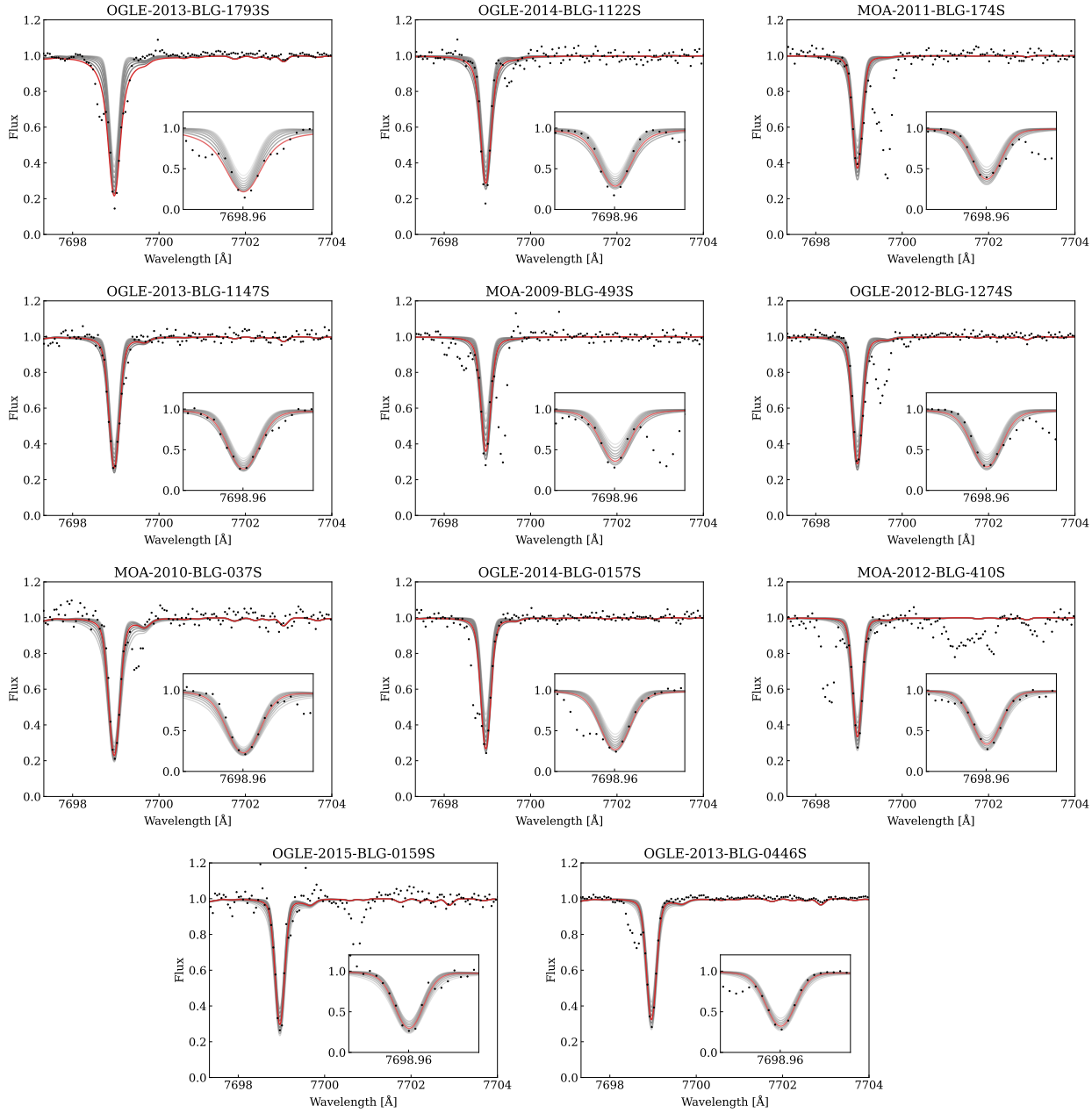

Figure 4.4: Abundance analysis of the outliers with *blended lines*, ordered such that the OGLE-2013-BLG-1793S correlate with the highest [K/Fe] and OGLE-2013-BLG-0446S correlate with the lowest [K/Fe] in this category.

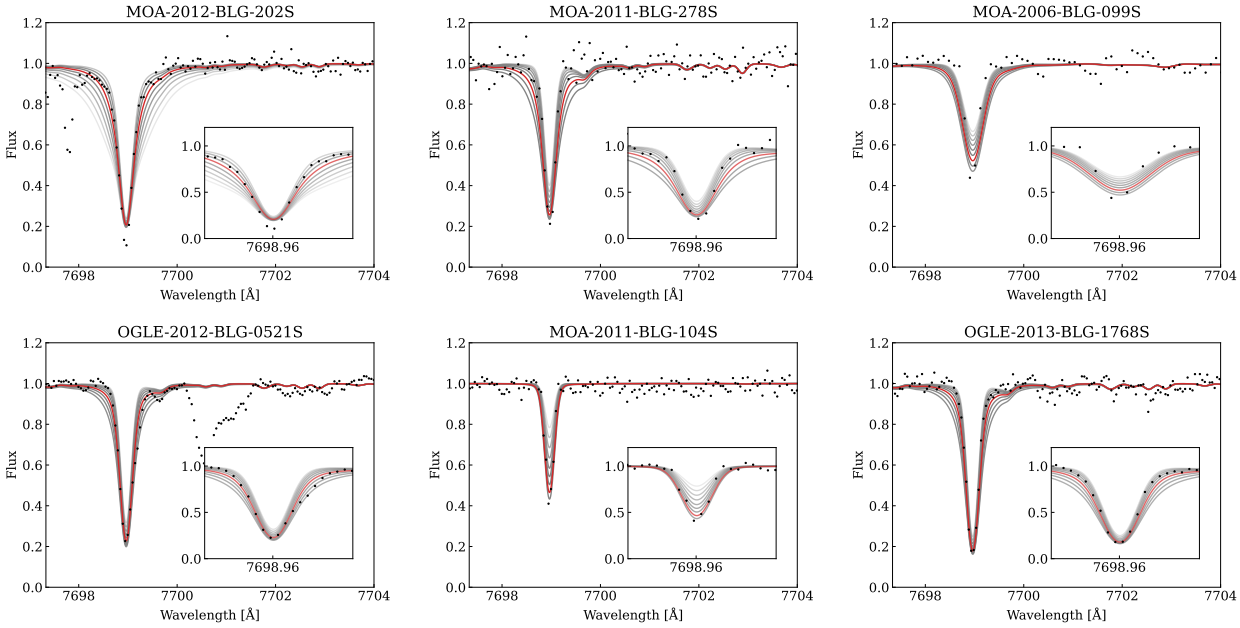

Figure 4.5: Abundance analysis of the outliers with *bad fits*, ordered such that the MOA-2012-BLG-202S correlate with the largest [K/Fe] and OGLE-2013-BLG-1768S correlate with the lowest [K/Fe] in this category.

4.2 α-elements

When evaluating the chemical evolution of a stellar population it is useful to use tracer elements, that is, elements that have well defined metallicity trends and/ or nucleosyntheitic processes. Hence it is useful to compare abundance ratios between elements to investigate if there is any coupling between the creation/ depletion of said elements. It turns out that α-elements are, as suggested by Woosley & Weaver (1995), useful tracers of chemical evolution due to the fact that they are believed to be mainly synthesized in massive stars, during various burning processes and/ or core-collapse supernovae.

A number of abundance ratios of K and various α-elements, such as oxygen (O), Titanium (Ti), Calcium (Ca), Silicon (Si) and Magnesium (Mg), have been computed, see figure 4.7. Similarly as in section 4.1 it is observed that the majority of the abundance ratios, with the slight exception of O, exhibit large dispersion compared to the disk-trends. Specifically, it is observed that the trends of Ca, Ti, Si and Mg in the disk(s) are not very visible in the bulge - the disk-trend is almost non-existent for mildly metal-poor to metal-rich stars in the bulge. This indicates, assuming the analysis is correct, that the nucleosynthetic coupling between Ca, Ti, Si, Mg and K might be different in the bulge compared to the disk(s). Contrary, the trend of O and K in the bulge seems to agree somewhat to the trend found in the disk(s), albeit the scattering of [K/O] is still large in comparison. This indicates that O would be the most suitable tracer element of K.

4.2.1 Outliers?

Similarly as in section 4.1 it is found, by observing the right column of figure 4.7, that a large portion of the dispersion observed in the [K/α] ratios are due to the previously defined *outliers*. The relative positions of these stars, with respect to trends of [α/Fe] and [Fe/H], are plotted in figure 4.6, to investigate if these stars exhibit any unexpected behaviour in the metallicity trends. It is found that, in the bulge, all the trends of α-elements reflect what is observed in the upper envelope of the trends found in the disk(s). But surprisingly, these *outliers* show little to no discrepancies in the metallicity trends of α-elements in the bulge, which hints at the notion that these stars might not be considered outliers for any elements but K.

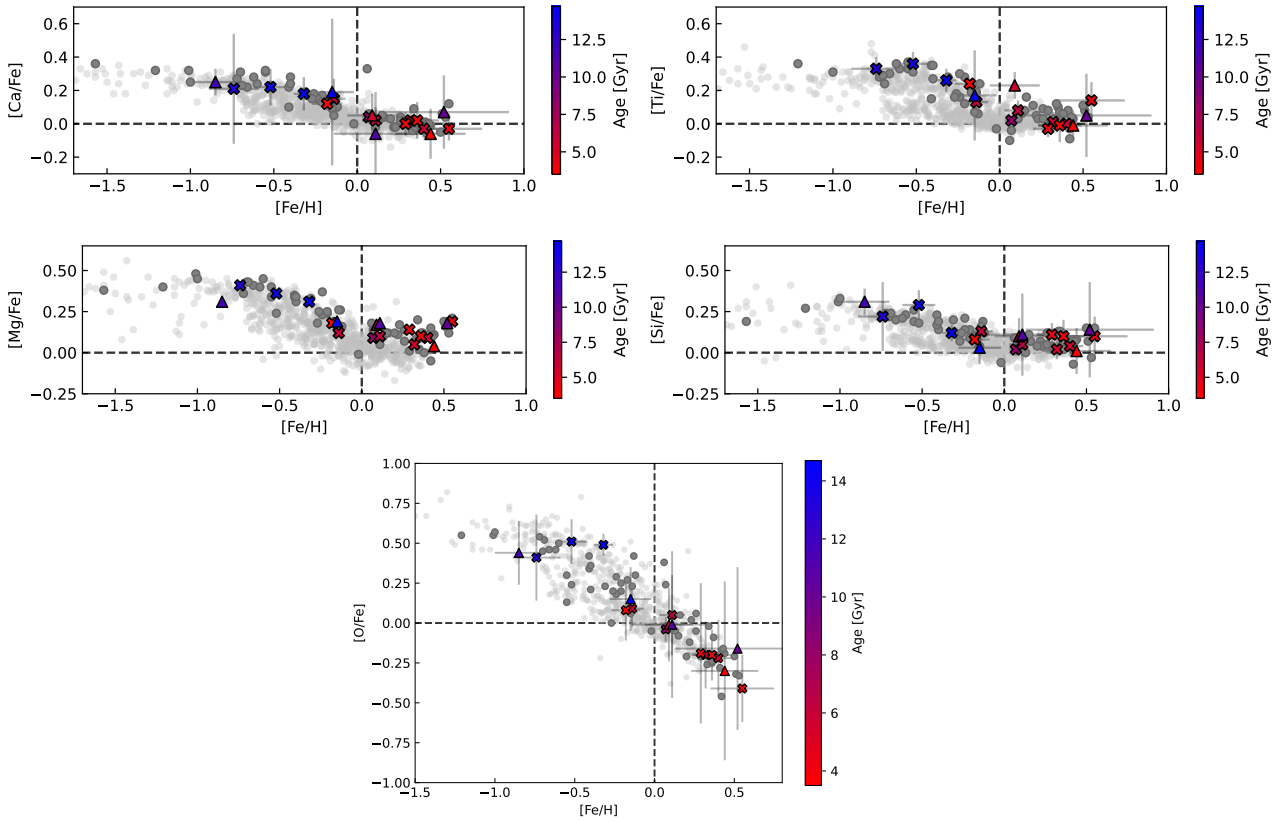

Figure 4.6: Metallicity trends of various α-elements. Grey and/ or color-mappend stars represent the bulge, while light-grey stars represent the disk(s). Specifically, stars that are color-mapped are *outliers*, where triangles represent *bad fits* and crosses represent *blended lines*. The abundances of the α-elements were previously determined by line synthesis in Bensby et al. (2017) & Bensby et al. (2021).

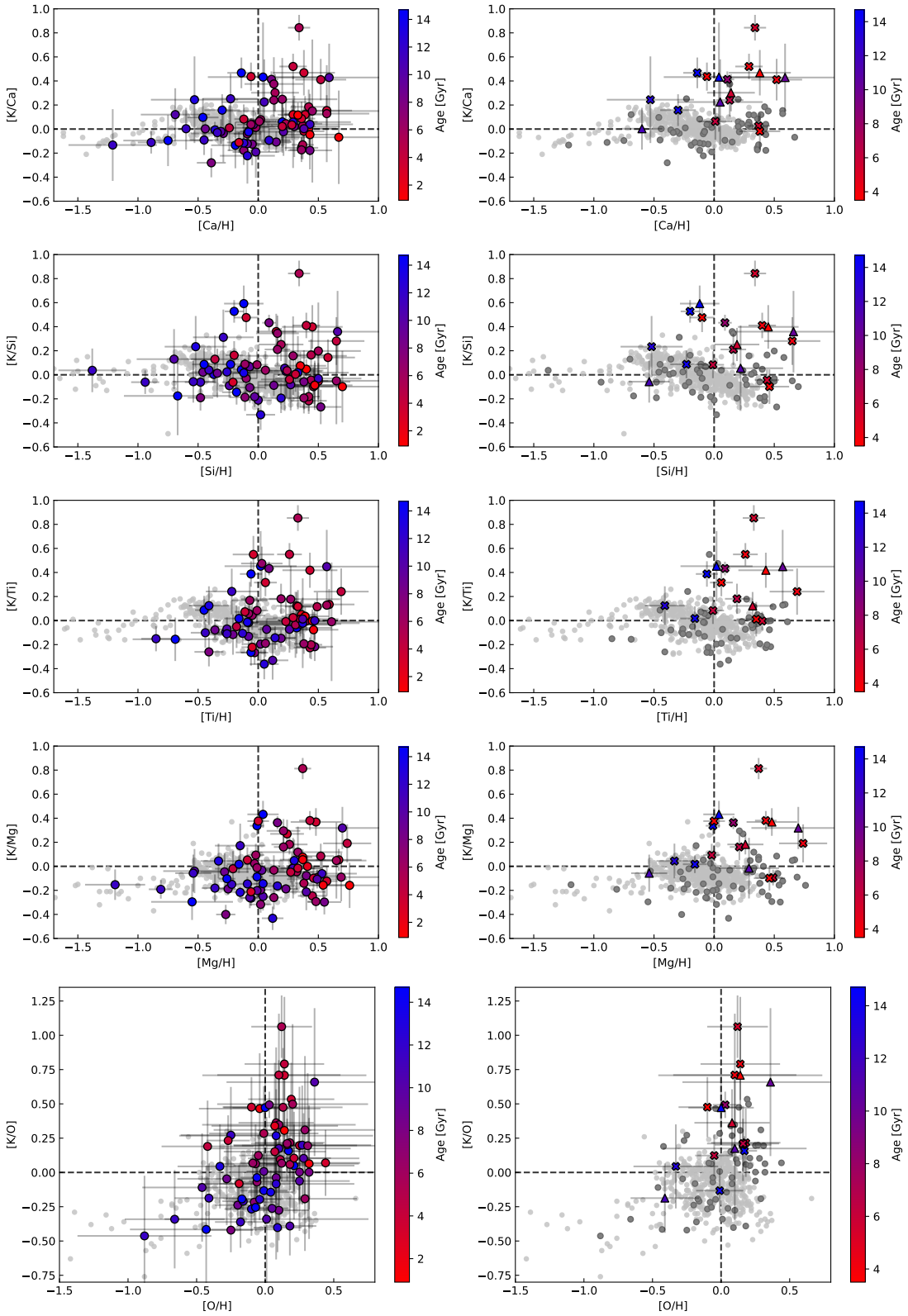

Figure 4.7: **Left:** [K/α] trends. **Right:** [K/α] trend with highlighted *outliers*. Color-scheme and markers is the same as in figure 4.6.

4.3 Outliers

The nature of why the *blended lines* are blended is currently unknown, but a few possible explanations exist. The simplest case would be to assume that the merging line were due to telluric contamination, but by inspecting figure 4.8, which compare a telluric spectrum three spectra exhibiting severely blended 7699 KI lines, it is observed that no significant telluric lines are present around the 7699 KI line. Thus, telluric contamination is deemed improbable.

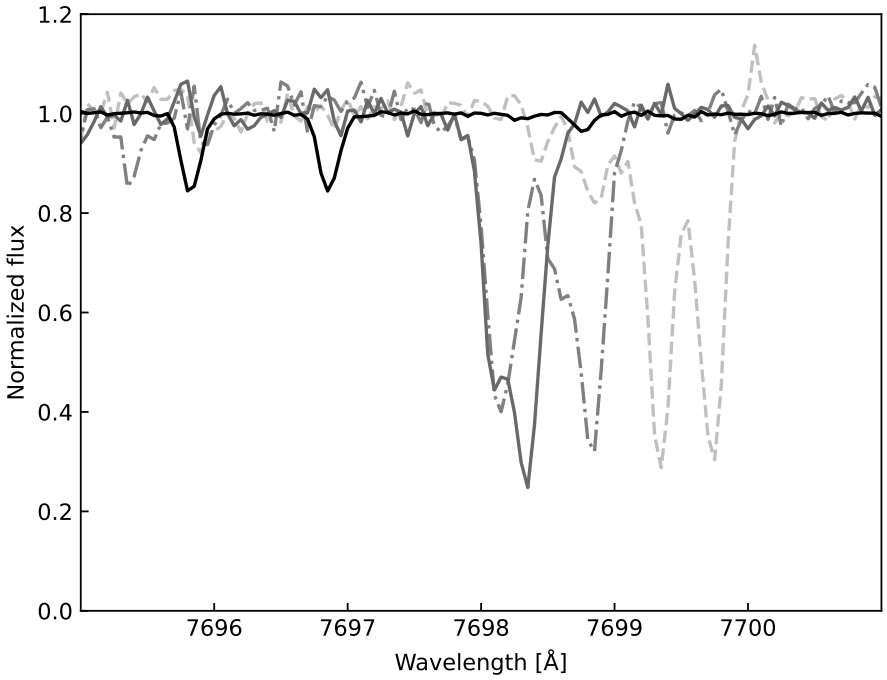

Figure 4.8: Normalized telluric spectrum, colored black, compared to normalized stellar spectra of MOA-2009-BLG-493S (solid line), MOA-2011-BLG-174S (dash-dotted line) and OGLE-2014-BLG-0157S (dashed line). It is important to note that comparisons such as this is done before any wavelength-corrections have been applied.

By inspecting figure 4.9 it is observed that the core of many of the merging lines do not align at a specific wavelength. There are two probable explanations of this - Diffuse Interstellar Bands (DIBs), which are absorption features due to interaction between photons and diffuse interstellar clouds, and/ or interstellar KI (Welty & Hobbs 2001). Both of which would produce similar anomalies, shifting the merging line back and forth around the 7699 KI line depending on the relative motion between the observed star and the cloud. However, it is currently unknown if the origin DIBs are due to dust or molecular/ atomic interaction, as only one out of several hundreds confirmed DIBs have been successfully identified (Geballe 2016). The width of DIBs vary significantly, where lines can have a Full-Width-Half-Maximum (FWHM) of as little as a few tens of mÅ (Herbig 1995), hence

it not impossible that the observed anomalies in the *blended lines* category are in fact due to DIBs or interstellar KI.

By the study of Maier et al. (2011) it is found that a possible carrier of the presumed DIB located around the 7699 KI line is the molecule H_2CCC, where the strength of the DIB is a function of reddening. See figure 4.10 for comparison of stars of different reddening. Similarly, by Strassmeier & Weber (2020) it is found that spectral features of interstellar K also is a function of reddening, and by observing figure 4.11 it is the observed that the spectral features of HD 1 exhibit striking similarities to some of the spectra observed in the *blended lines*.

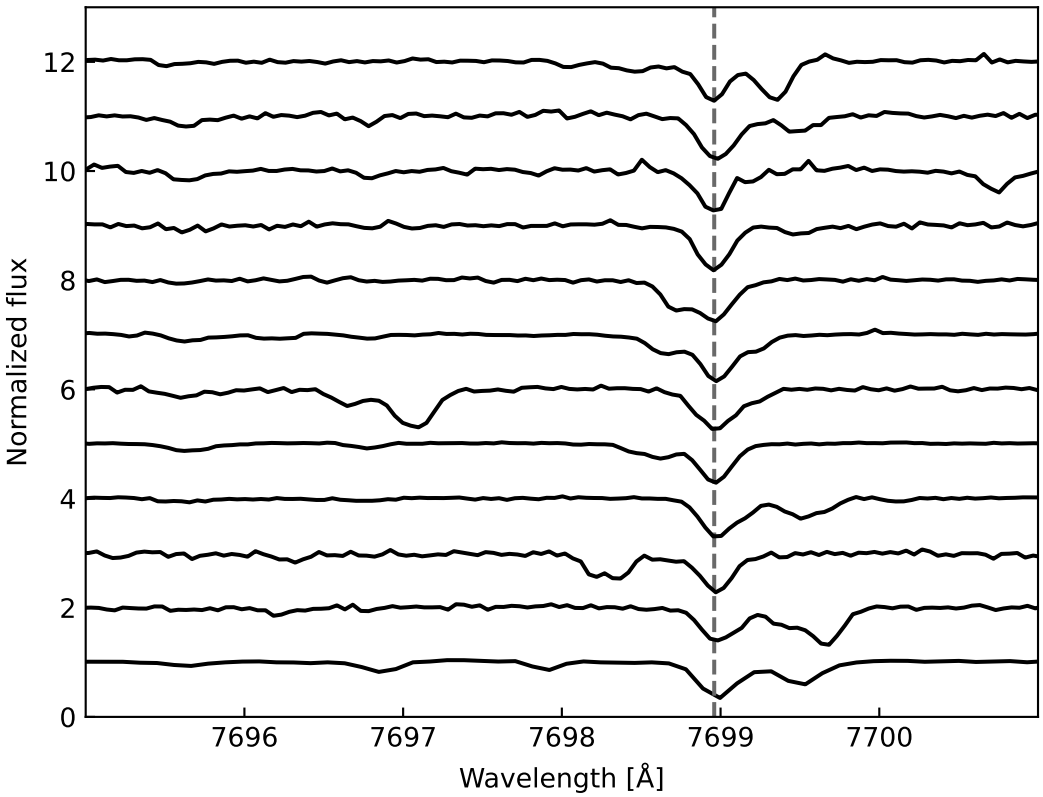

Figure 4.9: Illustration of where the merging line is located relative to the 7699 KI line, of spectrum from the *blended lines* category.

These spectral interactions might also be a reason why the synthetic spectra of the *bad fits* category do not fit the observed spectra very well - the core of the lines from the star and the DIB/ cloud might coincide, rendering the merge invisible and thus producing a deeper core of the spectral line than what pySME can predict. It is thus concluded that due to limitations of time and data no further information about what these blended lines are can be found during this study, but it is deemed probable that these spectral features contribute to a overestimation of the K abundance and that similarities between

the *outliers* and the figures of DIBs and interstellar K hint at the notion that these concepts might be the origin of the observed spectral features. But, future studies are required to confirm such notion.

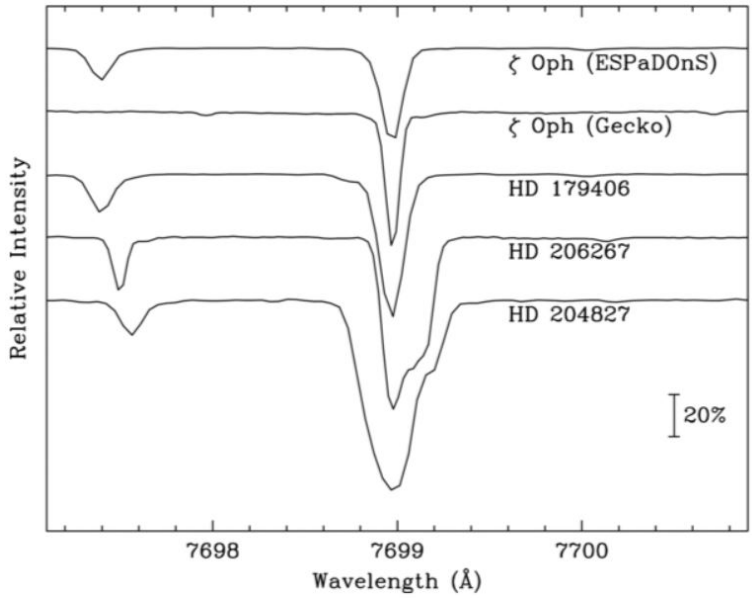

Figure 4.10: Figure from Maier et al. (2011), depicting how the strength of the DIB increase as a function of reddening (where ESPaDOnS and HD 203827 exhibit the least and most reddening, respectively). The spectra are aligned on their most prominent spectral feature.

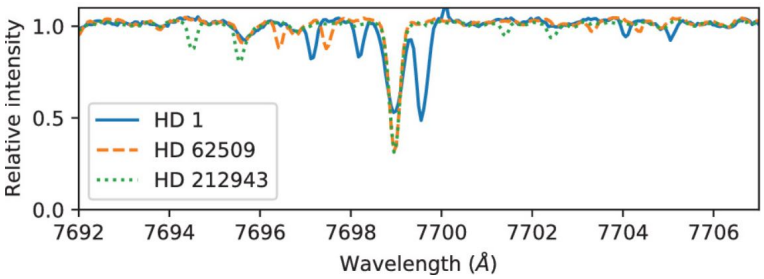

Figure 4.11: Figure from Strassmeier & Weber (2020), depicting three spectra from the Henry Draper catalog, where HD 1 exhibit absorption lines from interstellar cloud containing K, with a non-zero relative velocity to HD 1, hence another 7699 KI emerge.

4.4 Age dependence

As per figure 4.1 and figure 4.7, and due to the unknown nature of the blended lines, no obvious age dependence is observed for any of the trends. A slight exception being [K/O], where a small trend of increasing [K/O] as a function of age is observed. Though it is

worth noting that a significant number of the seemingly K-enhanced stars are of ages 8 Gyr or younger.

Chapter 5

Discussion

Overall the analysis of this report is assumed reasonable, as precautions of the results have been statistically estimated and *outliers* have been thoroughly investigated. Though a few points of interest are further discussed below.

5.1 Sophisticated Search Algorithms

Being able to predict the chemical abundance of distant galaxies, and thus the chemical evolution of the Universe as a whole, require accurate abundances of elements in our galactic neighbourhood (the Milky Way). Thus it is of crucial importance to make accurate measurements when determining the abundance of any element. As previously stated this report employed an iterative method of finding the optimal abundance, that is, a set of discreet abundance-values were iteratively evaluated until a good fit had been found. This is both time consuming, since the machine keeps iterating even if a good fit is found early on in the process, and somewhat inaccurate as the true abundance might be located between any two discreet values. Although some precautions to combat this inaccuracy were applied during the analysis, by the fitting and minimization of ψ. These two arguments render this method rather in-efficient.

The author suggest that a method akin to a random walk should be used instead. This will speed up the program by possibly minimizing the number of iterations used per spectrum as well as finding more accurate abundances and margins of error. See resources such as Nocedal & Wright (2006) for ideas of how to construct such sophisticated search algorithms.

5.2 Potassium Enrichment

As to what process might be responsible for the enrichment of K, assuming the abundance analysis is correct, in the bulge is beyond the authors knowledge. Though a few ideas have

be brought to light, and is summarised in the following sections.

5.2.1 AGB Outflows and Stellar Winds

It is commonly assumed that only supernovae significantly contribute to the enrichment of the interstellar medium (ISM), but as per Iliadis et al. (2016) it is found that stellar outflows and/ or winds of the super-Asymptotic-Giant-Branch (SAGB) stars have non-negligible contributions to the enrichment of the ISM. It is in fact found that these processes are crucial to include when trying to reproduce the K abundance in our solar system.

Studies on the K-enhanced globular cluster NGC 2419 (Kemp et al. 2018) also suggest that the enrichment of K might be due to stars of the SAGB as these stars only need an temperature increase of 10 to 20 MK at the bottom of the envelope, making it possible to produce K by depleting sodium (Na) (Prantzos et al. 2017). The K-rich outer layers of the star would then be deposited onto its low-mass companion stars by stellar winds and/ or outflows, thus making the low-mass companions K-enhanced.

5.2.2 Other Polluters

As per Kemp et al. (2018) it is deemed not probable that low-mass stars contribute to the enrichment of K, as temperature increases of 100 to 200 MK is needed for production of K to start, thus ruling out all core/ shell burning processes for stars below the SAGB. Though it is hypothesized that a polluter candidate is pair-instability super-nova (PISN) (Carretta et al. 2013). These events are unique to extremely massive population III stars and involve the total destruction of the star, leaving no remnant behind. Hence the yield from these events are massive, albeit rare.

The enhanced levels of K in the globular cluster NGC 2419 might come from just one PISN event (Kemp et al. 2018), thus affecting all stars in the cluster at once. The K-trend of the bulge lay somewhere between what is observed in the disk(s) and NGC 2419, indicating that no one such events enriched the entire bulge simultaneously. This is somewhat reasonable as the bulge is $\sim$100 times larger than NGC 2419 (Ryden & Peterson 2020), making it improbable for one PISN event to enrich the entire bulge at once. But maybe several such event have occurred in the distant past, suggesting that the enrichment of K might be location dependent and /or dependent on the galactic environment.

5.3 Blended Lines revisited

Due to the lack of time no hands-on investigation of the origin of the *blended lines* have been made. But, if time would permit, a few things come to mind which would be interesting to investigate. Firstly, a inspection of when, or rather *where*, the observation of each star were made would be very interesting to see if the wavelength-shift of the merging line, relative to the 7699 KI line, correlate with any heliocentric correction needed to account

for the motion of the Earth relative to the Sun. This correction can vary by as much as 30 km/s, see appendix B for calculation, which is equivalent to a Doppler-shift of ~ 0.5 Å. This wavelength-shift is very much in line with the range observed of the merging line in figure 4.9.

Secondly, assuming the heliocentric correction have already been applied by Bensby, it would be of great interest to investigate if the direction (relative to the 7699 KI line), and possibly the magnitude, of the wavelength-shift of the merging line can be correlated with certain galactic longitudes. As an illustrative example, assuming clockwise rotation of the bulge, all spectra which exhibit merging lines at longer wavelengths relative to 7699 KI should be located at galactic longitudes less than 0. And likewise, spectra which exhibit merging lines at shorter wavelengths relative to 7699 KI should be located at galactic longitudes larger than 0.

One could also investigate the nature of these potential clouds by observing fast rotating B-stars in the Galactic Bulge, due to the fact that B-stars have very few spectral lines. And sufficiently fast rotation would smear the spectral lines such that the spectra observed would mostly be due to the interstellar medium. If such observations are made and reasonable results are found then one could subtract these lines from the stellar spectra and thus obtain a more accurate abundance analysis.

Chapter 6

Conclusion

A comprehensive abundance analysis of 77 low- to intermediate- mass stars in the Galactic Bulge have been performed. Using a method of line synthesis the metallicity trend [K/Fe] along with trends of α-elements ([K/α]) have been computed and evaluated. It was found that the almost all trends in the bulge exhibit large dispersion from what is found in the disk(s) and no overall age dependence was found for any of the trends. The only slight exception being [K/O], where the trend of the bulge and disk(s) was almost similar and a slight age dependence of increasing [K/O] as a function of decreasing age was observed.

However, the dispersion of all trends was found to be mainly due to a sample of stars which exhibit unexpected spectral features - the 7699 KI line was blended by a unknown spectral line of varying strength. The cause of this anomaly have been investigated, and possible explanations could be either due to Diffuse Interstellar Bands (DIBs) or interstellar KI. Both of which would produce similar anomalies as observed in figure 4.9. It is deemed probable these spectral features contribute to a overestimation, and thus the dispersion, of K-trends in the Galactic Bulge.

It is thus concluded that the results of this report is intriguing, but uncertain, and further studies are required to confirm if the implied enrichment of K in the bulge is true or simply due to interactions between spectral lines of different origin.

Bibliography

Amarsi, A. M., Lind, K., Osorio, Y., et al. 2020, A&A, 642, A62

Andrievsky, S. M., Spite, M., Korotin, S. A., et al. 2010, A&A, 509, A88

Arcones, A. & Thielemann, F.-K. 2023, , 31, 1

Asplund, M., Grevesse, N., & Sauval, A. J. 2005, in Astronomical Society of the Pacific Conference Series, Vol. 336, Cosmic Abundances as Records of Stellar Evolution and Nucleosynthesis, ed. I. Barnes, Thomas G. & F. N. Bash, 25

Bensby, T., Adén, D., Meléndez, J., et al. 2011, A&A, 533, A134

Bensby, T., Feltzing, S., Gould, A., et al. 2017, A&A, 605, A89

Bensby, T., Feltzing, S., Johnson, J. A., et al. 2010, A&A, 512, A41

Bensby, T., Feltzing, S., & Oey, M. S. 2014, A&A, 562, A71

Bensby, T., Gould, A., Asplund, M., et al. 2021, A&A, 655, A117

Bensby, T., Yee, J. C., Feltzing, S., et al. 2013, A&A, 549, A147

Bergemann, M. & Nordlander, T. 2014, arXiv e-prints, arXiv:1403.3088

Bernstein, R., Shectman, S. A., Gunnels, S. M., Mochnacki, S., & Athey, A. E. 2003, in Instrument Design and Performance for Optical/Infrared Ground-based Telescopes, ed. M. Iye & A. F. M. Moorwood, Vol. 4841, International Society for Optics and Photonics (SPIE), 1694 – 1704

Carretta, E., Gratton, R. G., Bragaglia, A., et al. 2013, ApJ, 769, 40

Dekker, H., D'Odorico, S., Kaufer, A., Delabre, B., & Kotzlowski, H. 2000, in Society of Photo-Optical Instrumentation Engineers (SPIE) Conference Series, Vol. 4008, Optical and IR Telescope Instrumentation and Detectors, ed. M. Iye & A. F. Moorwood, 534–545

Geballe, T. R. 2016, in Journal of Physics Conference Series, Vol. 728, Journal of Physics Conference Series, 062005

Gray, D. F. 2021, The Observation and Analysis of Stellar Photospheres, 4th edn. (Cambridge University Press)

Gustafsson, B., Edvardsson, B., Eriksson, K., et al. 2008, A&A, 486, 951

Herbig, G. H. 1995, ARA&A, 33, 19

Iliadis, C., Karakas, A. I., Prantzos, N., Lattanzio, J. C., & Doherty, C. L. 2016, ApJ, 818, 98

Karakas, A. I. & Lattanzio, J. C. 2014, , 31, e030

Kemp, A. J., Casey, A. R., Miles, M. T., et al. 2018, MNRAS, 480, 1384

Kupka, F. G., Ryabchikova, T. A., Piskunov, N. E., Stempels, H. C., & Weiss, W. W. 2000, Baltic Astronomy, 9, 590

Lind, K., Melendez, J., Asplund, M., Collet, R., & Magic, Z. 2013, A&A, 554, A96

Maier, J. P., Walker, G. A. H., Bohlender, D. A., et al. 2011, ApJ, 726, 41

Nocedal, J. & Wright, S. J. 2006, Numerical Optimization, 2nd edn. (New York, NY, USA: Springer)

Norregaard, C. 2018, Potassium in the Galactic thin and thick discs, Student Paper

Prantzos, N., Charbonnel, C., & Iliadis, C. 2017, A&A, 608, A28

Reggiani, H., Amarsi, A. M., Lind, K., et al. 2019, A&A, 627, A177

Rutten, R. J. 2003, Radiative Transfer in Stellar Atmospheres

Ryden, B. & Peterson, B. M. 2020, Foundations of Astrophysics (Cambridge University Press)

Strassmeier, K. G. & Weber, M. 2020, Astronomische Nachrichten, 341, 983

Takeda, Y. 2020, arXiv e-prints, arXiv:2001.04588

Tominaga, N., Umeda, H., & Nomoto, K. 2007, ApJ, 660, 516

Valenti, J. A. & Piskunov, N. 1996, , 118, 595

Vogt, S. S., Allen, S. L., Bigelow, B. C., et al. 1994, in Instrumentation in Astronomy VIII, ed. D. L. Crawford & E. R. Craine, Vol. 2198, International Society for Optics and Photonics (SPIE), 362 – 375

Wehrhahn, A., Piskunov, N., & Ryabchikova, T. 2023, A&A, 671, A171

Welty, D. E. & Hobbs, L. M. 2001, , 133, 345

Woosley, S. E. & Weaver, T. A. 1995, , 101, 181

Zasowski, G., Schultheis, M., Hasselquist, S., et al. 2019, ApJ, 870, 138

Zhang, H. W., Gehren, T., Butler, K., Shi, J. R., & Zhao, G. 2006, A&A, 457, 645

Zhao, G., Mashonkina, L., Yan, H. L., et al. 2016, ApJ, 833, 225

Appendix A

Plots of stellar fits and Chi^2

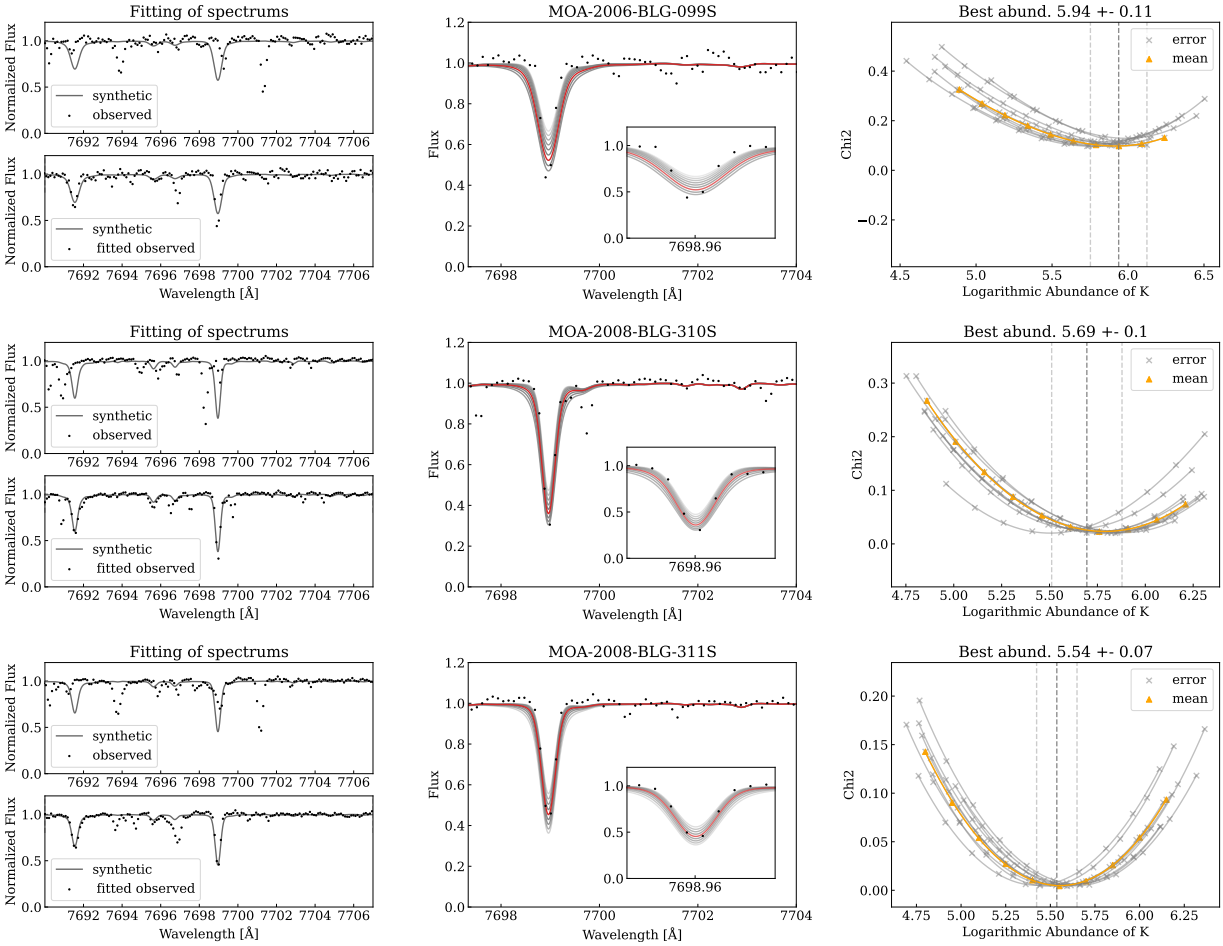

Figure A.1: Abundance analysis of the 7699 KI line.

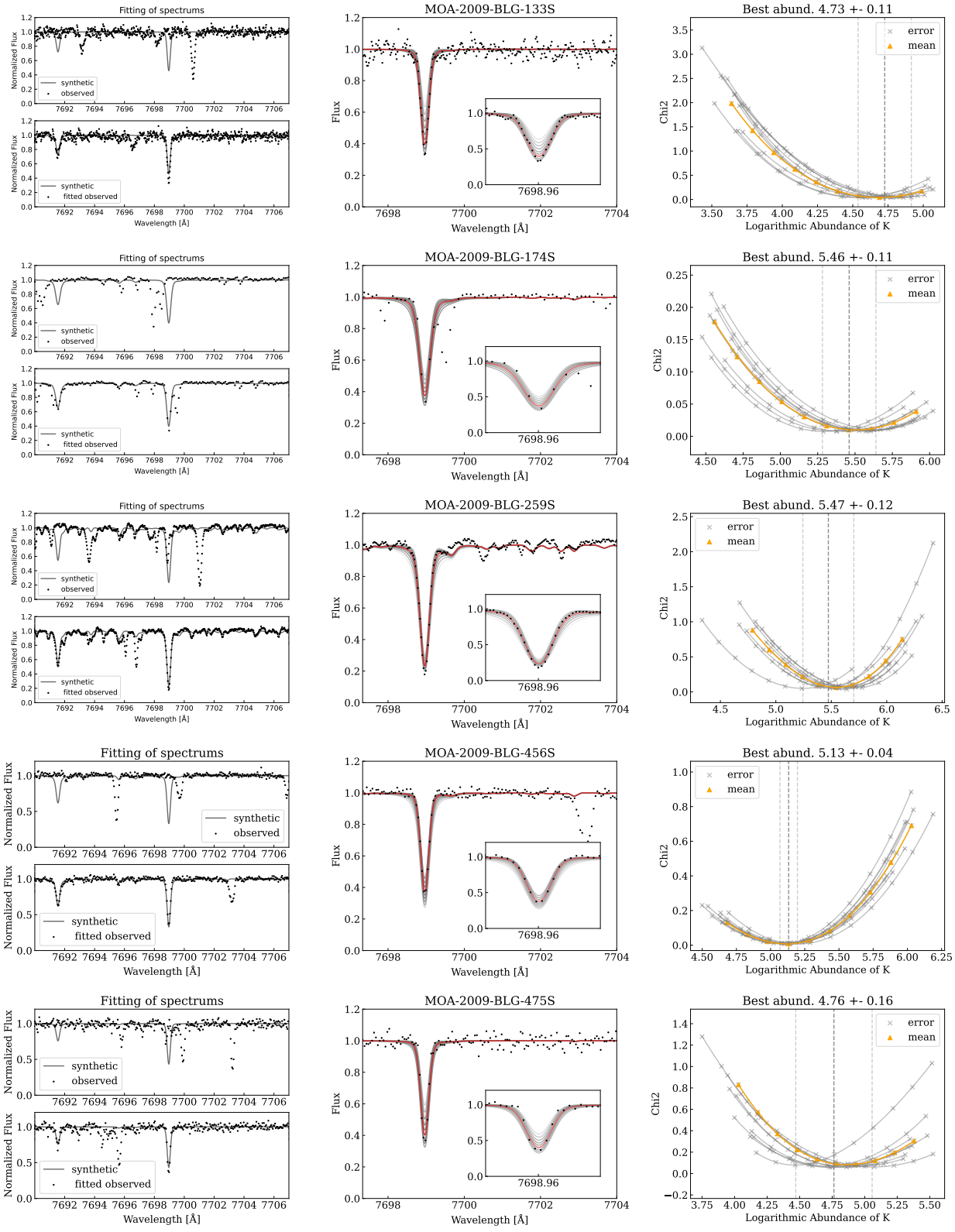

Figure A.2: Abundance analysis of the 7699 KI line.

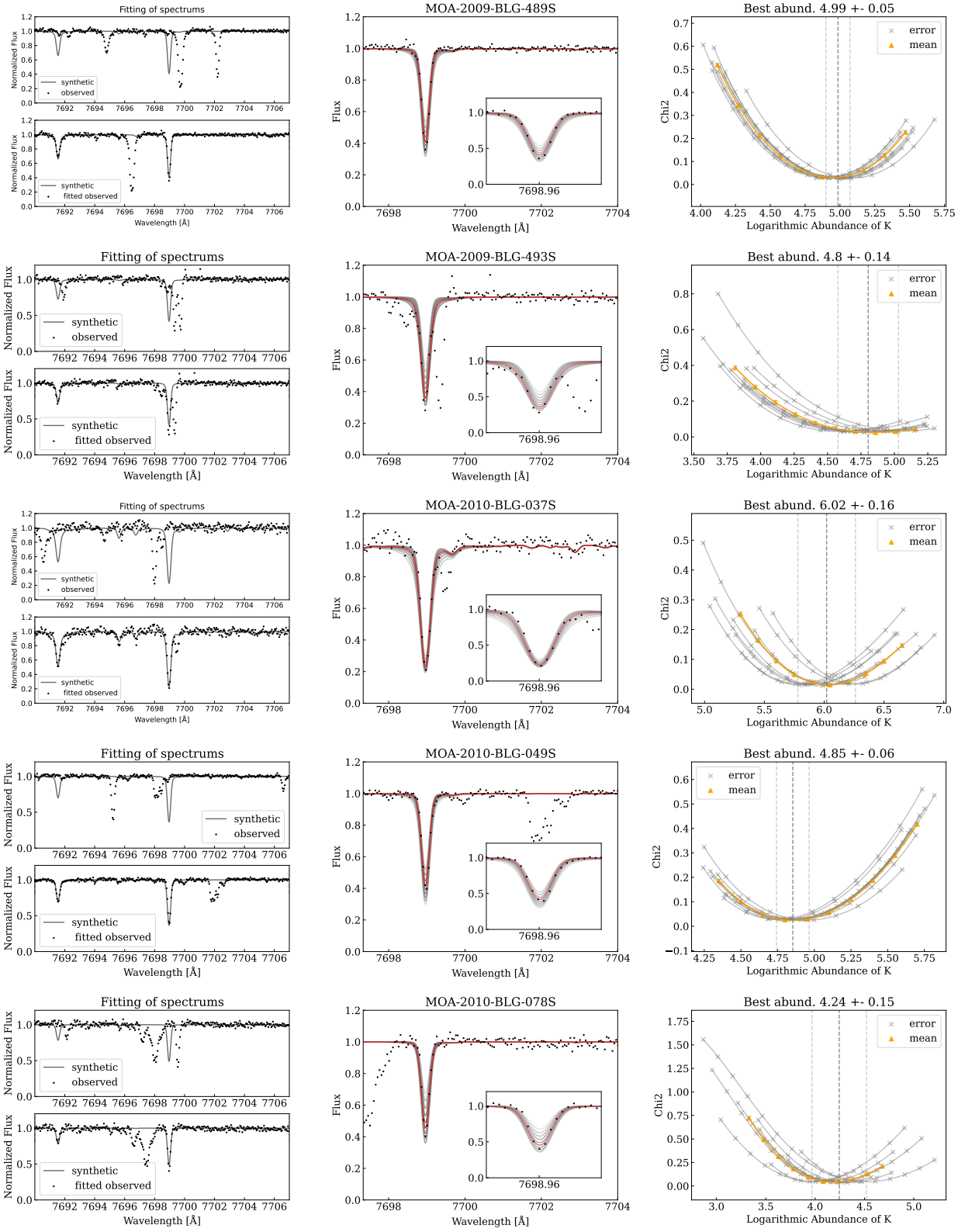

Figure A.3: Abundance analysis of the 7699 KI line.

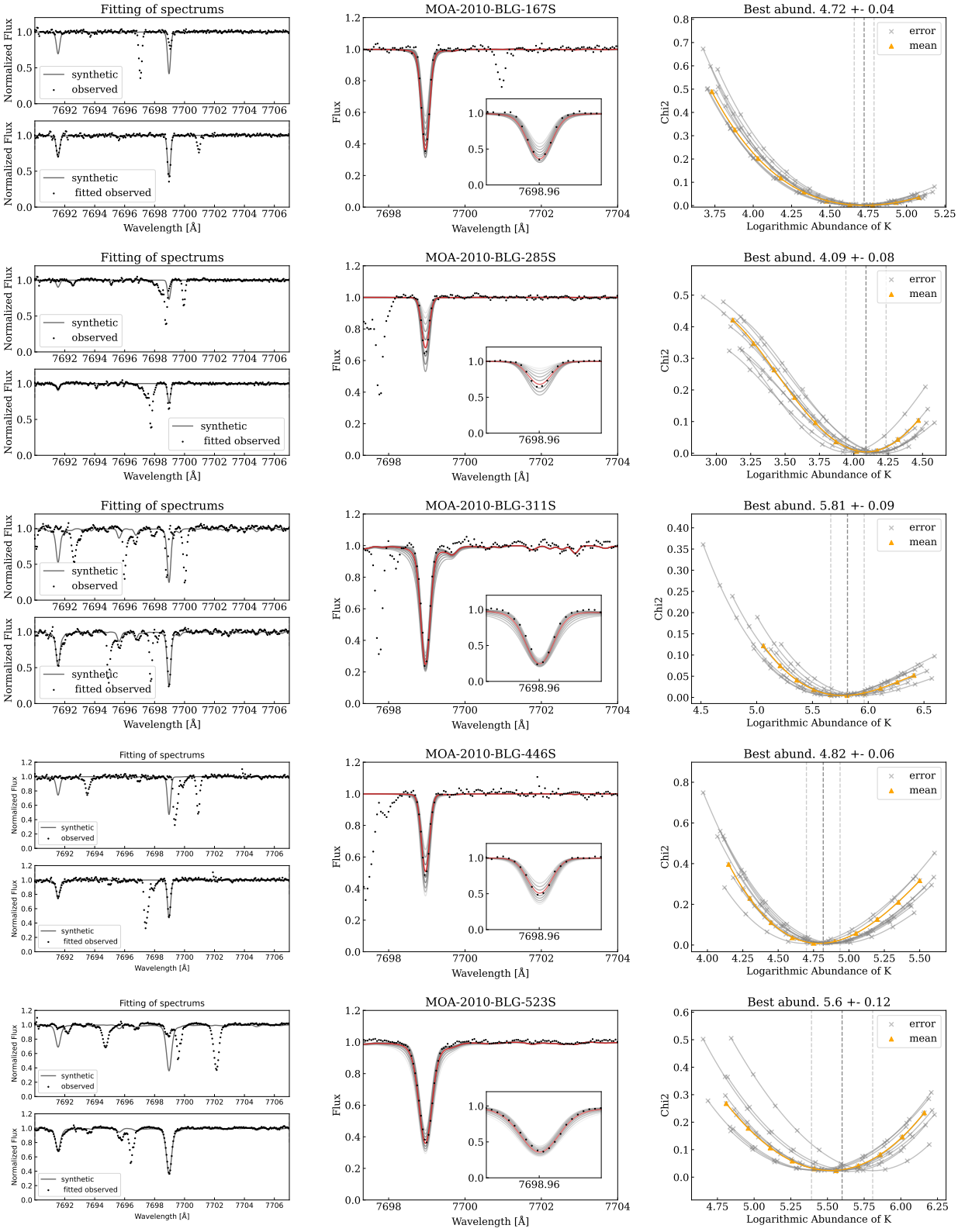

Figure A.4: Abundance analysis of the 7699 KI line.

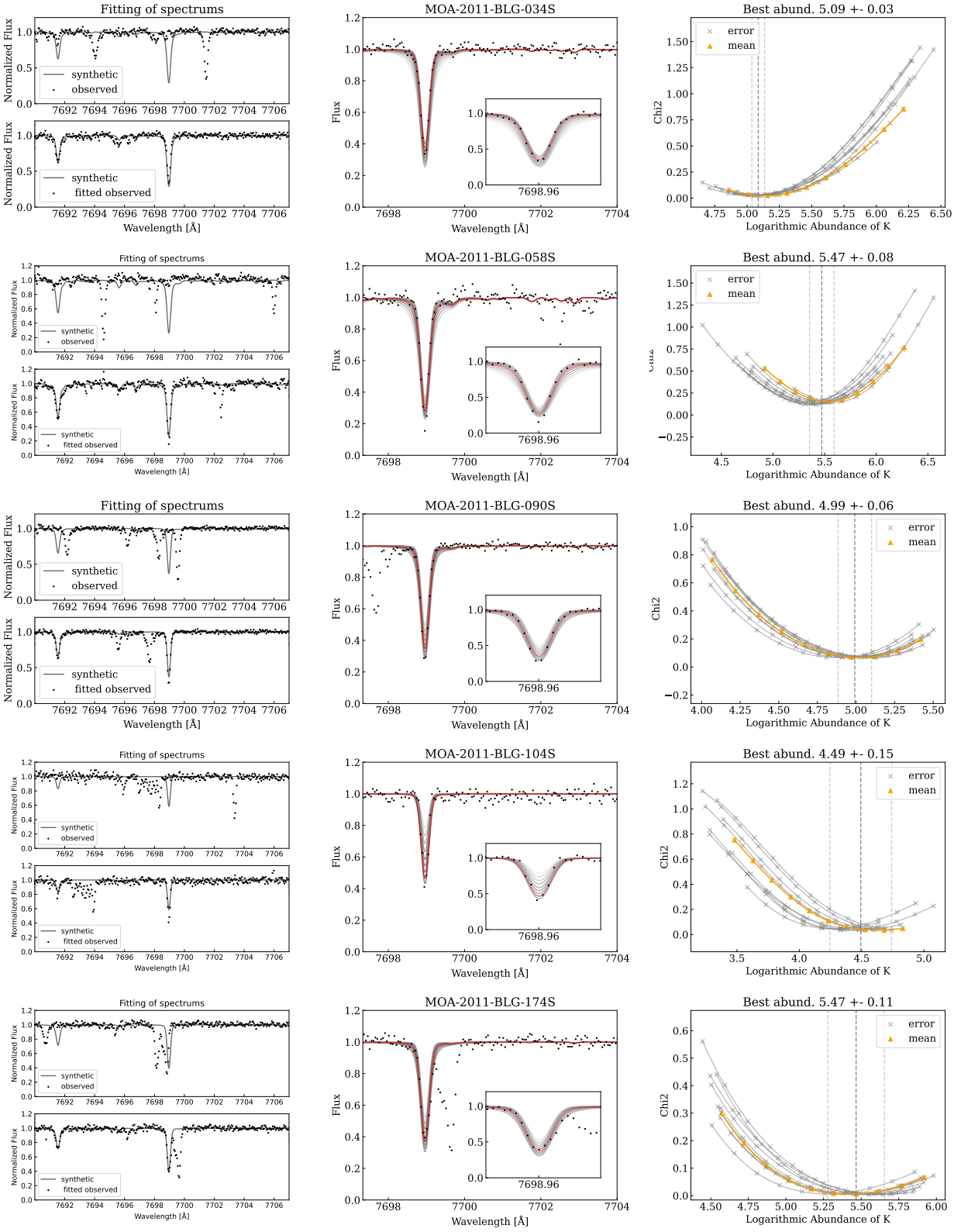

Figure A.5: Abundance analysis of the 7699 KI line.

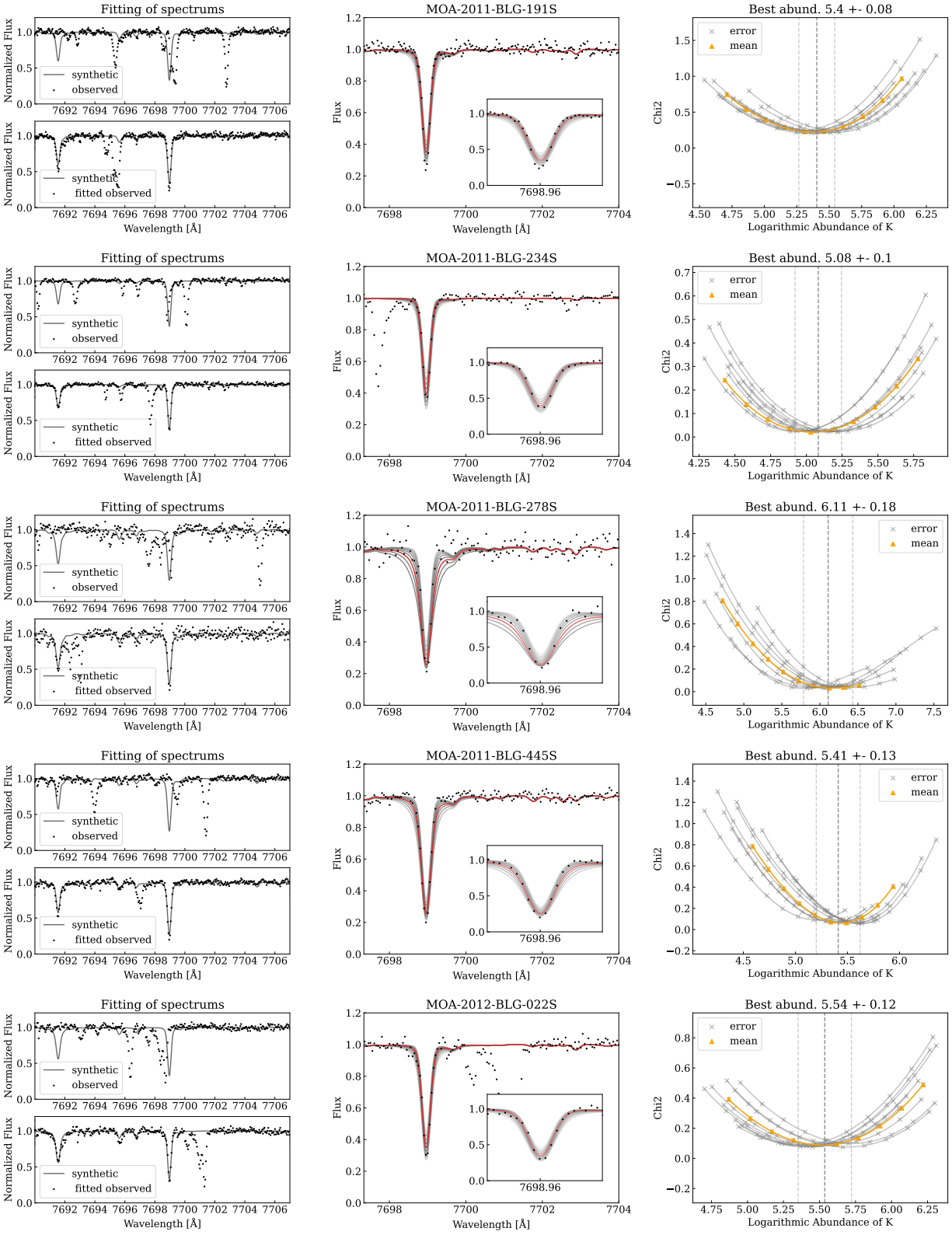

Figure A.6: Abundance analysis of the 7699 KI line.

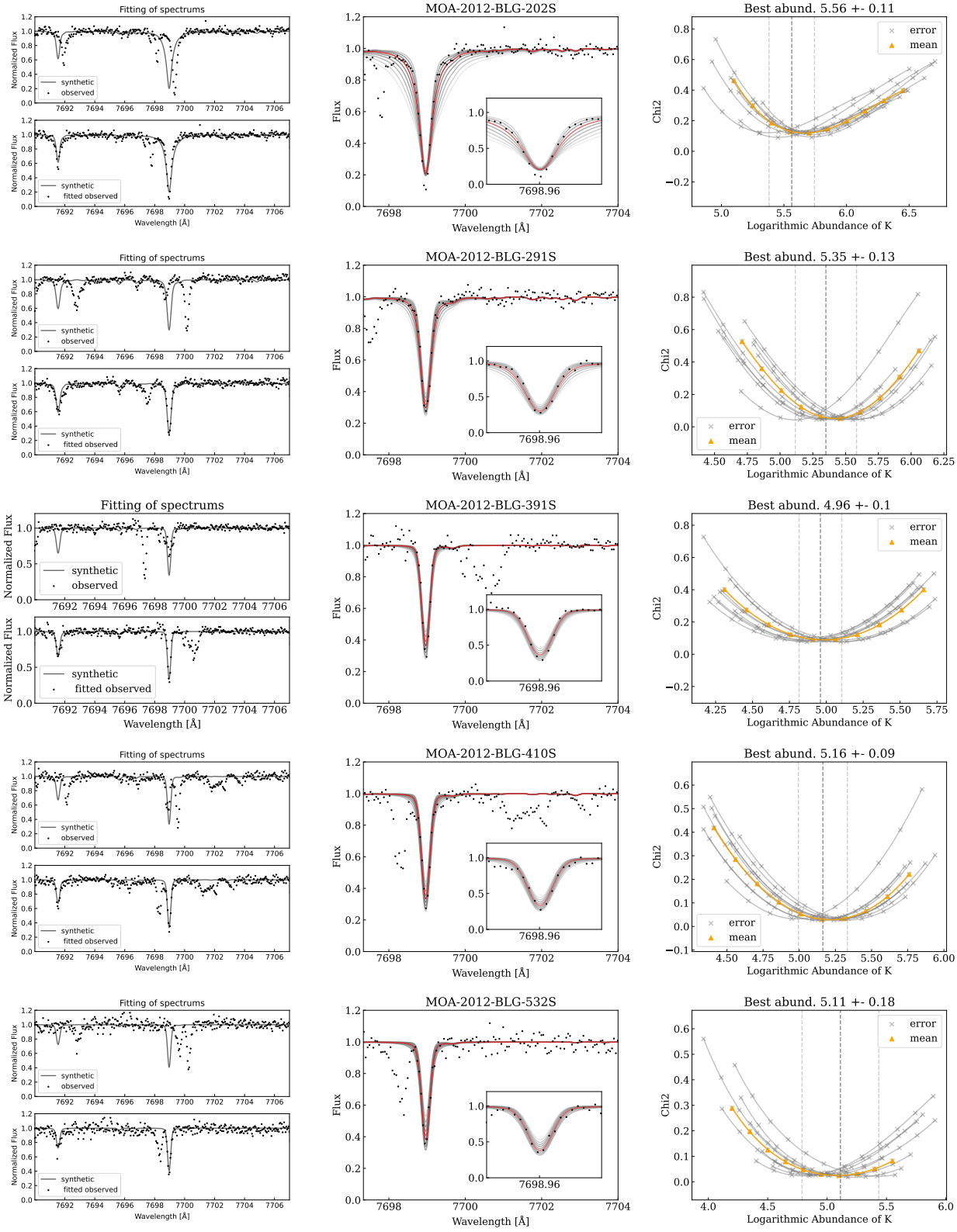

Figure A.7: Abundance analysis of the 7699 KI line.

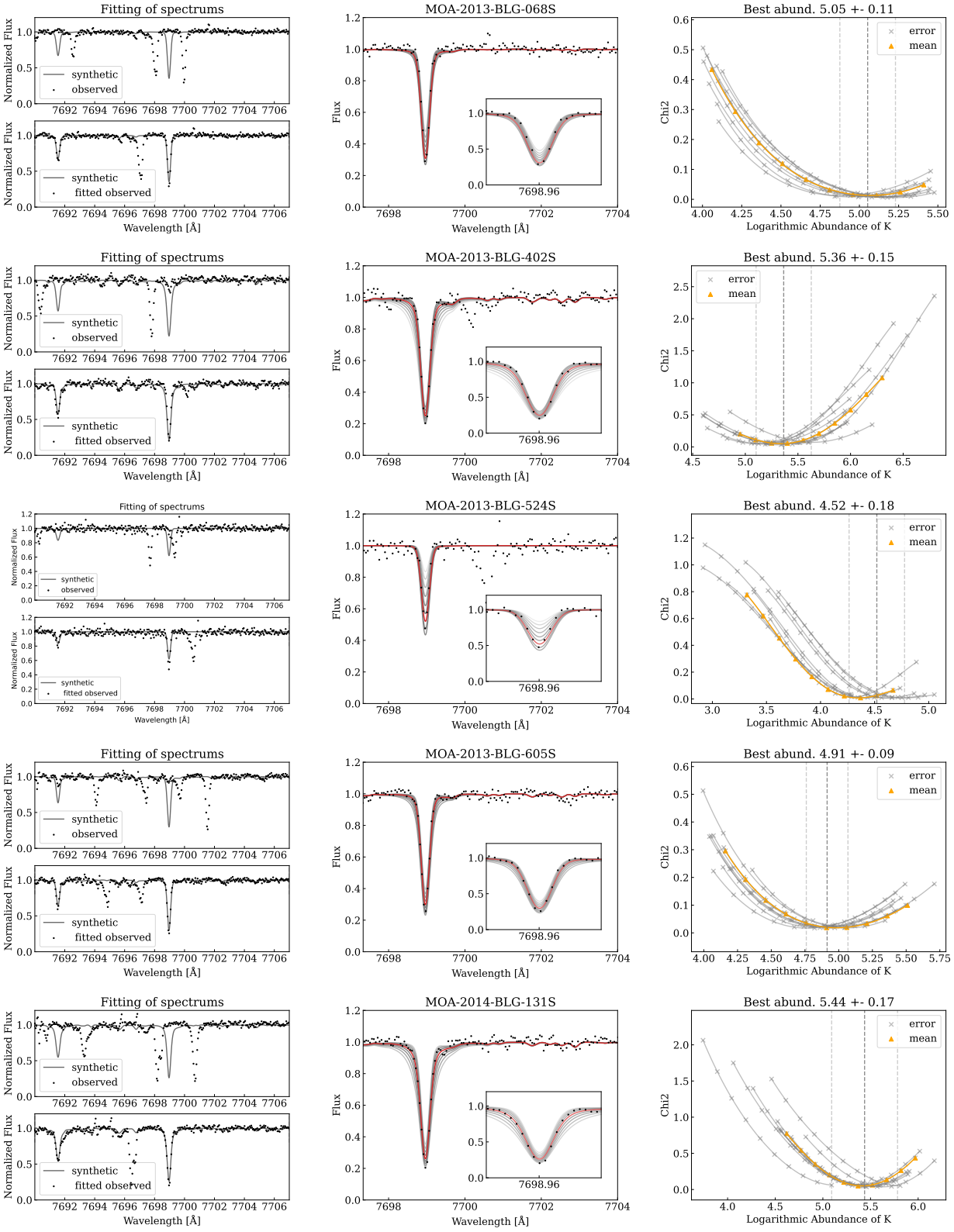

Figure A.8: Abundance analysis of the 7699 KI line.

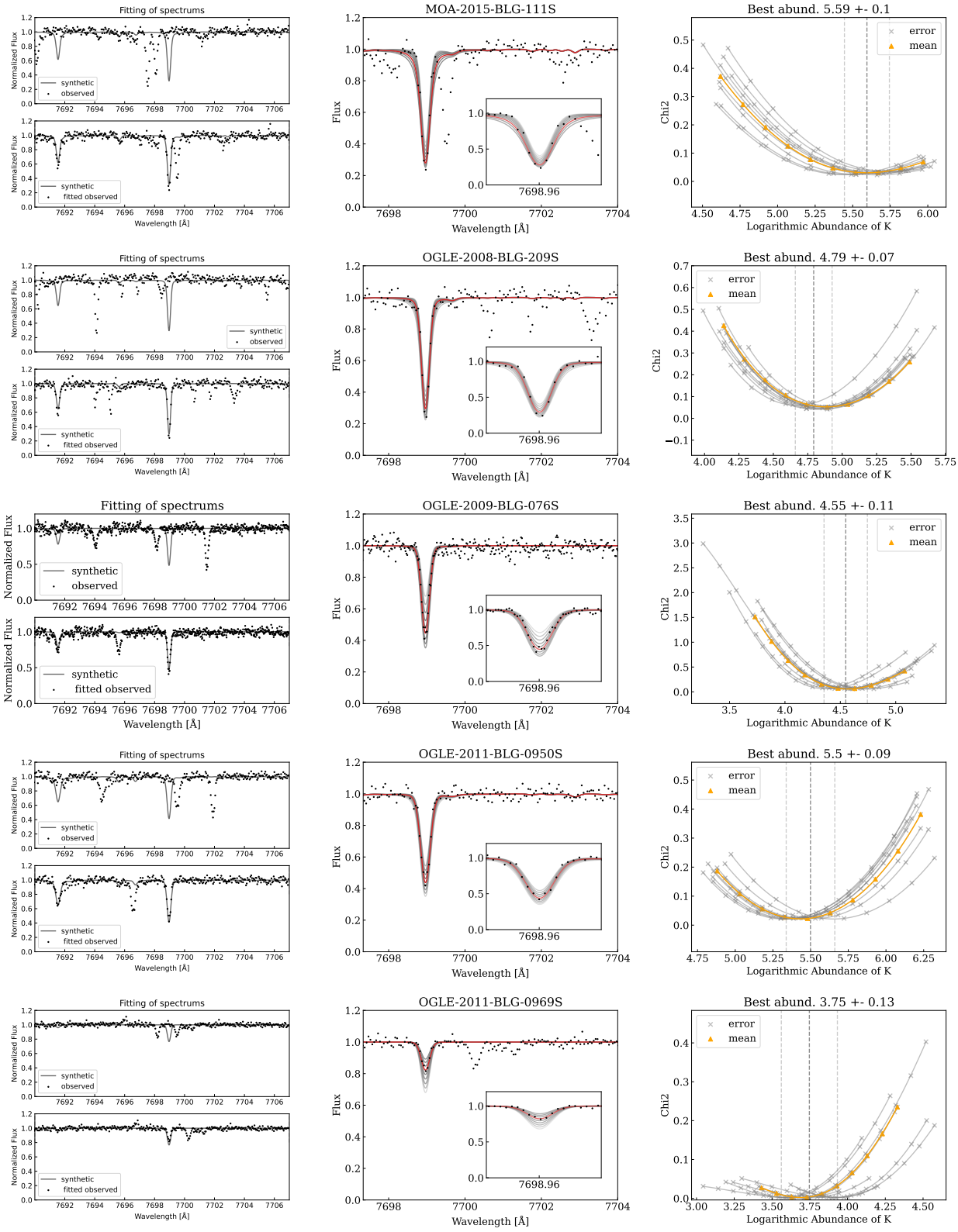

Figure A.9: Abundance analysis of the 7699 KI line.

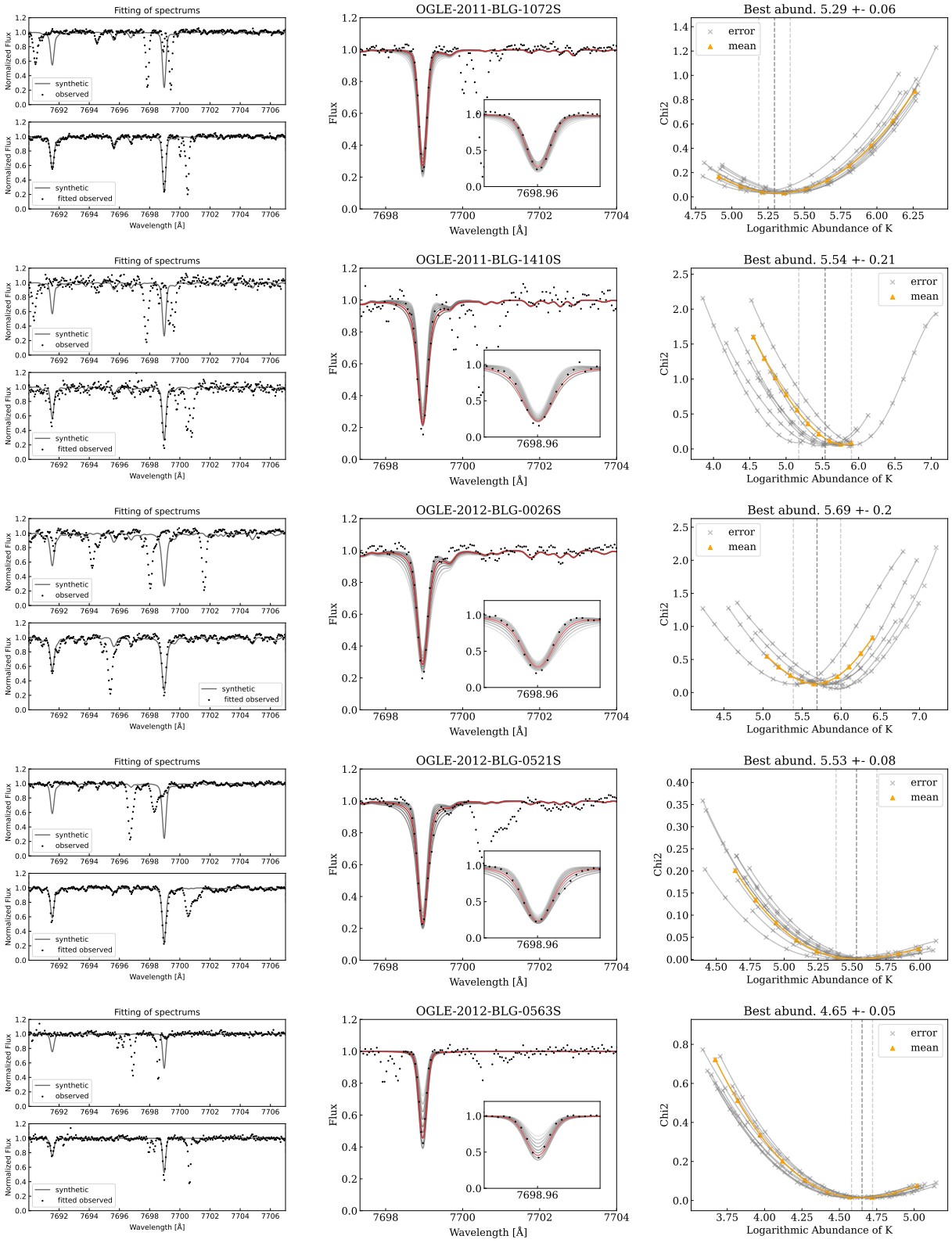

Figure A.10: Abundance analysis of the 7699 KI line.

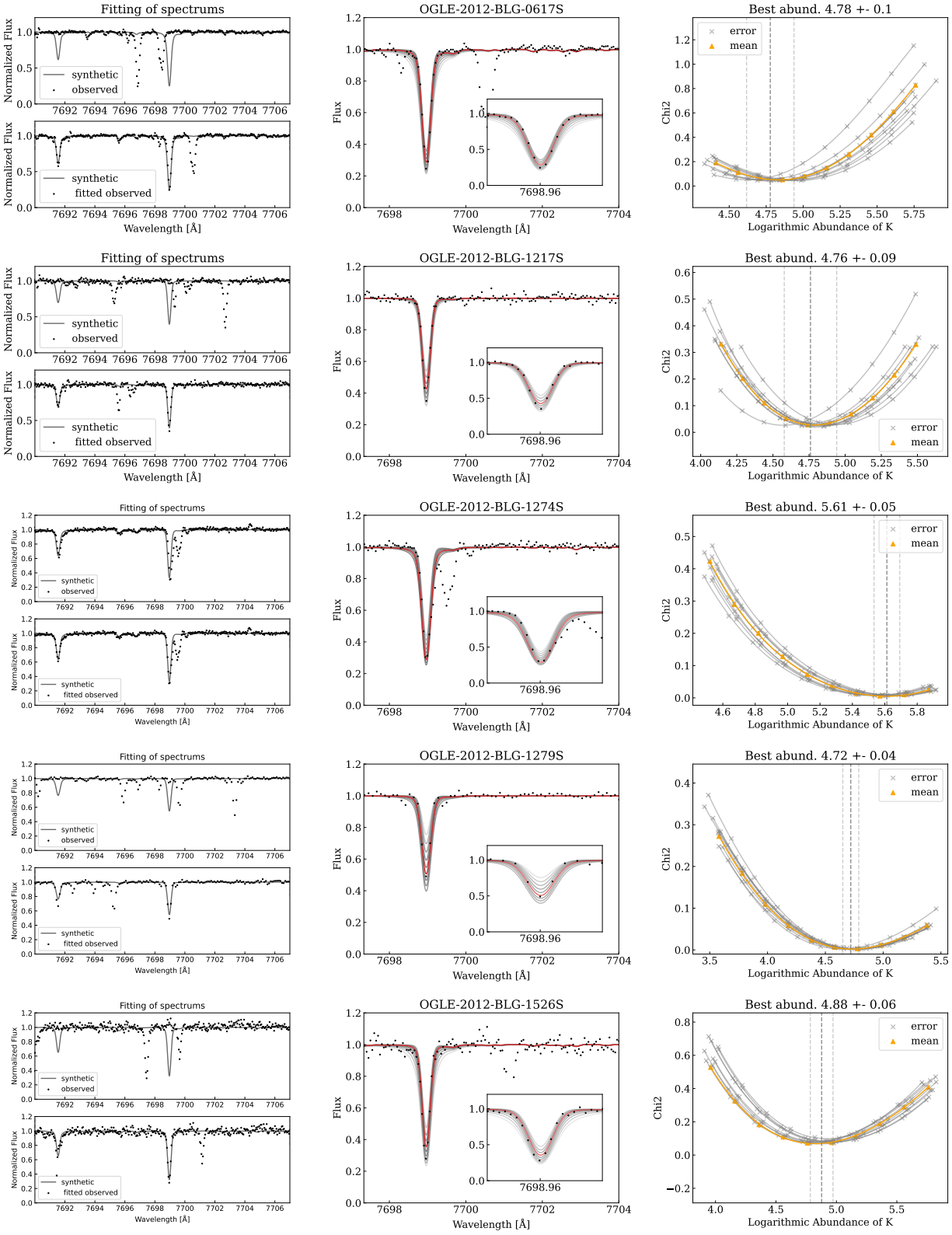

Figure A.11: Abundance analysis of the 7699 KI line.

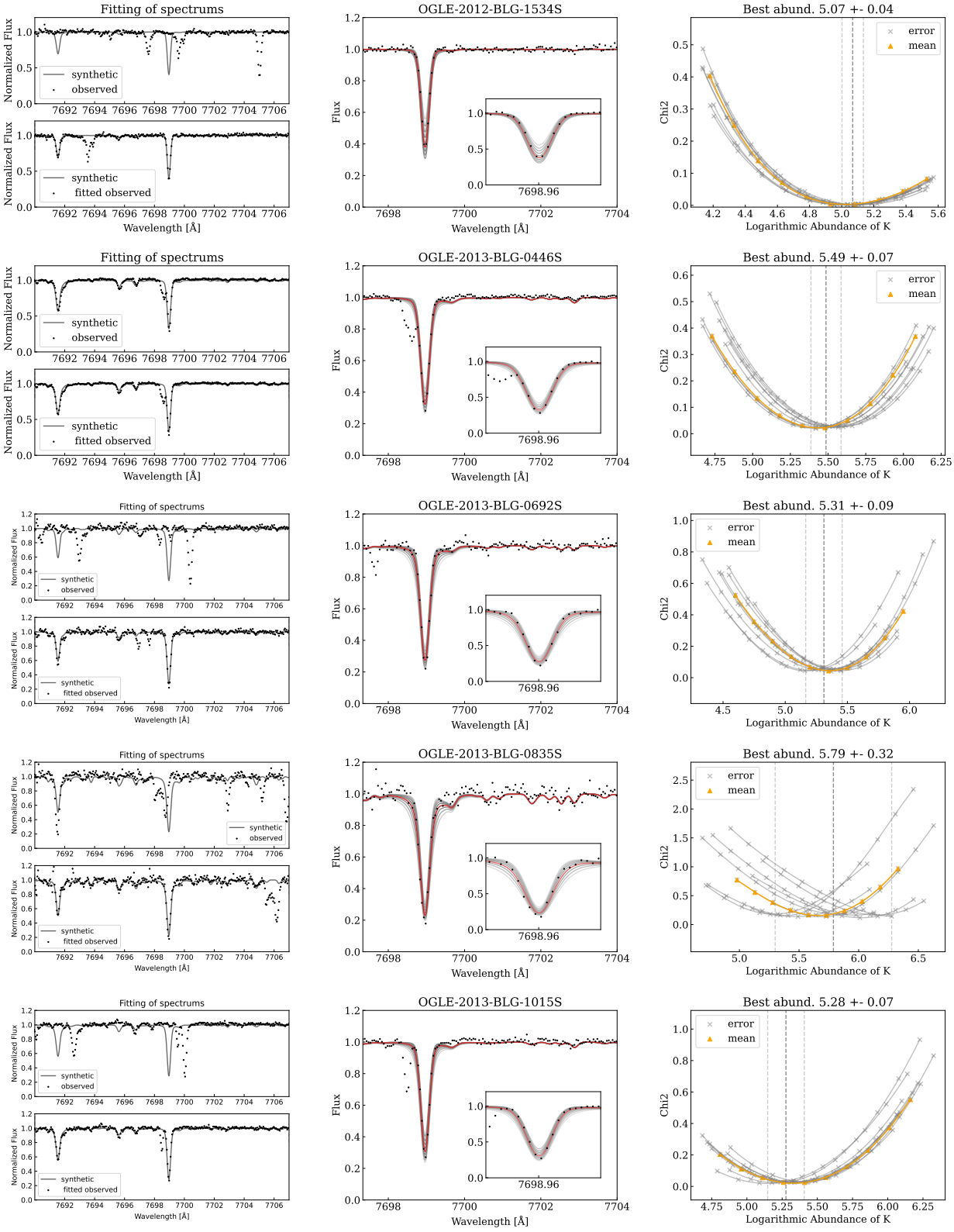

Figure A.12: Abundance analysis of the 7699 KI line.

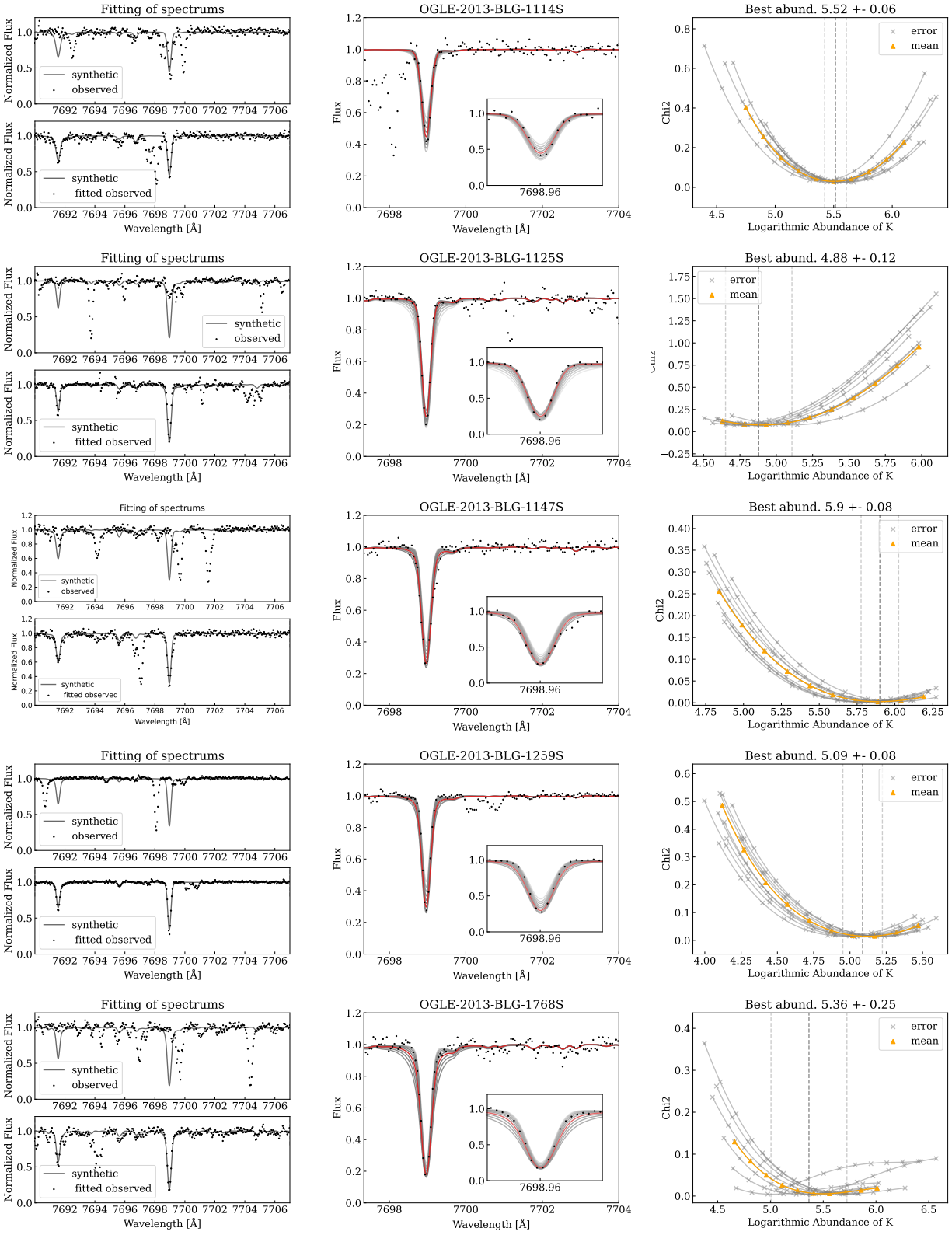

Figure A.13: Abundance analysis of the 7699 KI line.

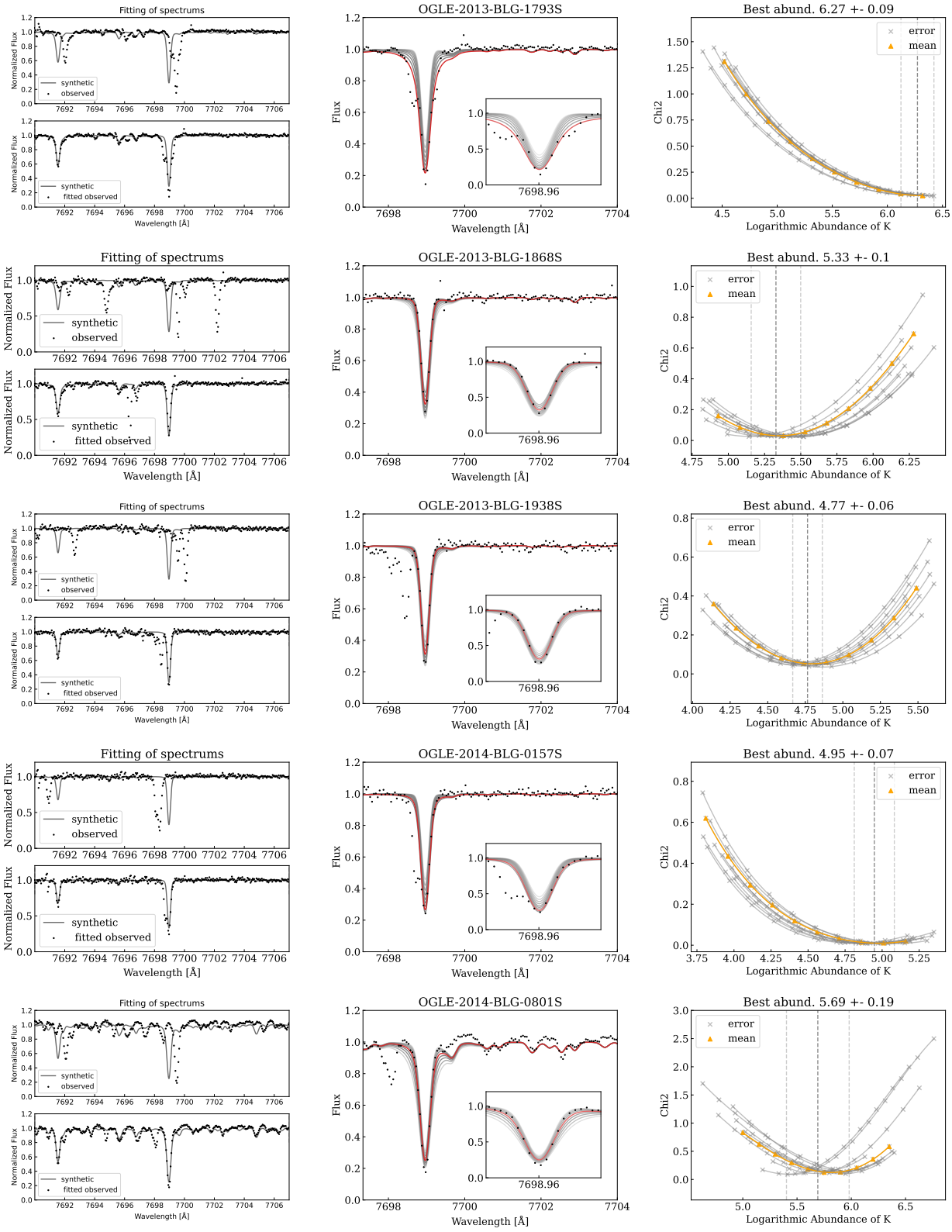

Figure A.14: Abundance analysis of the 7699 KI line.

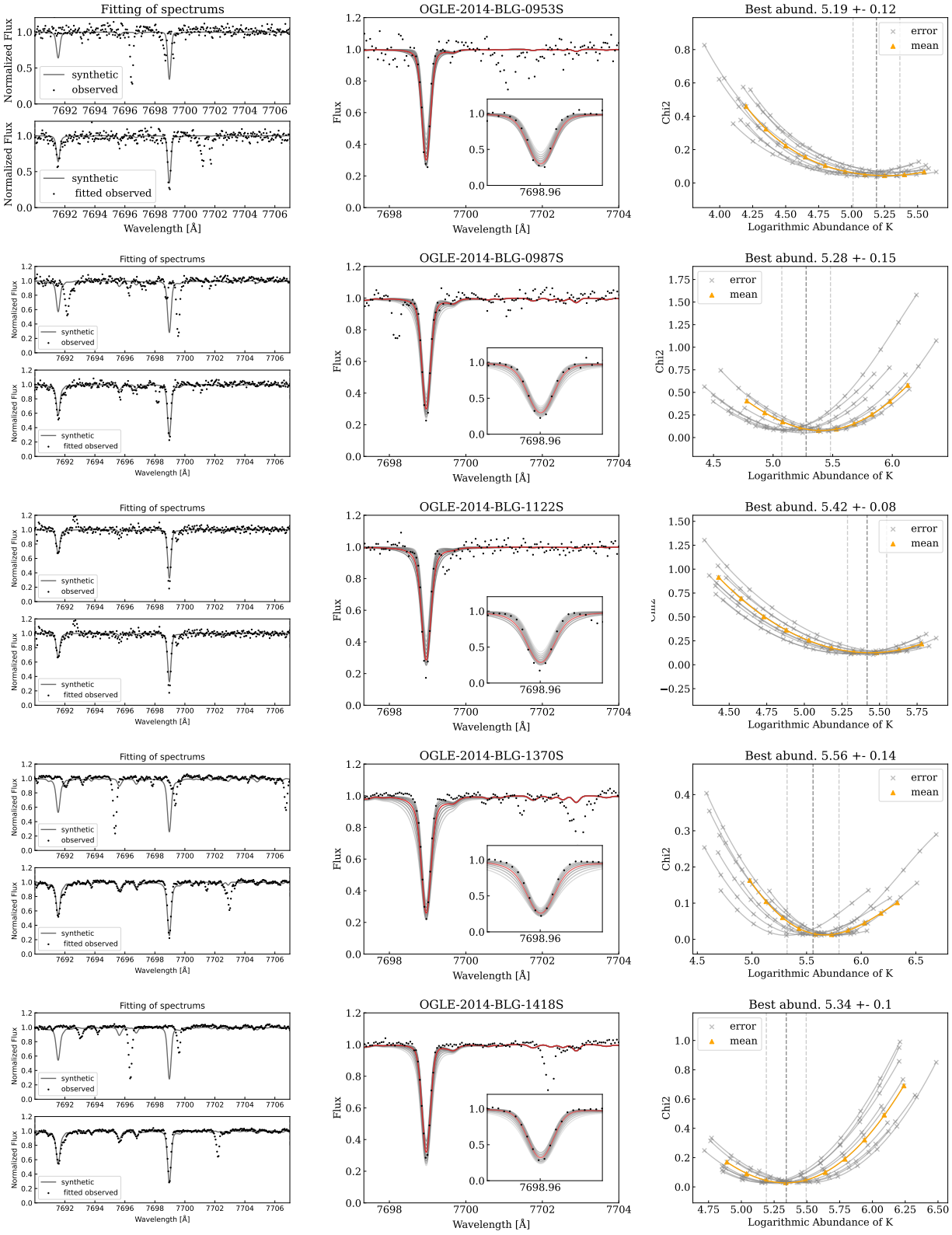

Figure A.15: Abundance analysis of the 7699 KI line.

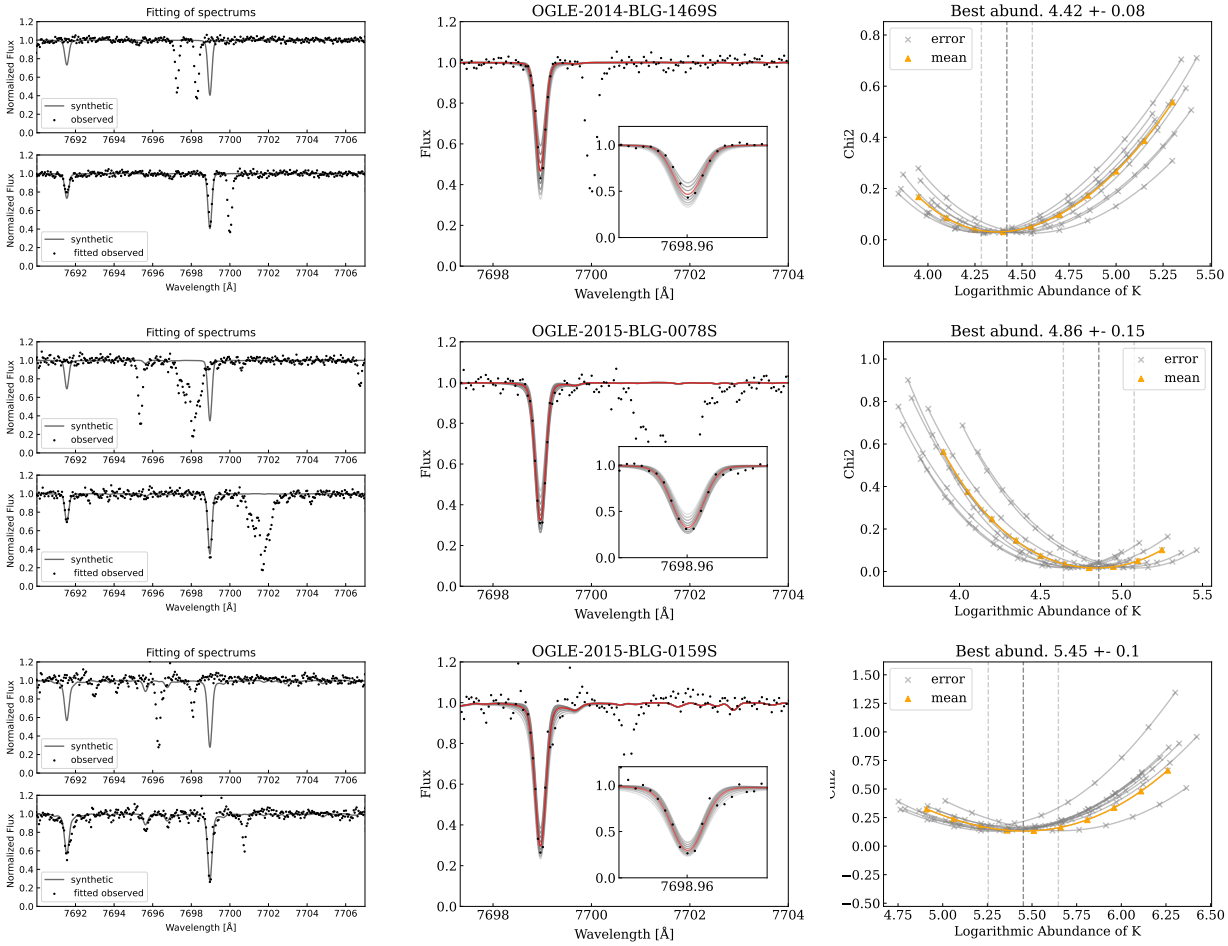

Figure A.16: Abundance analysis of the 7699 KI line.

Appendix B

Derivations

B.1 Abundance Ratios

The abundance data from *tablea2* and the Bensby et al. (2014) disk sample are on the format A(X) or $[X_1/X_2]$, that is, no particle number densities are used in any of the calculations. Hence, calculating [K/Fe] is trivial, see equation B.1.

$$[\mathrm{K/Fe}] = \mathrm{A(K)} - \mathrm{A(K)}_\odot - [\mathrm{Fe/H}] \tag{B.1}$$

Similarly, the ratios $[\mathrm{K}/\alpha]$ and $[\alpha/\mathrm{H}]$ are derived in equation B.2 and B.3.

$$\begin{aligned}[\mathrm{K}/\alpha] = [\mathrm{K/Fe}] - [\alpha/\mathrm{Fe}] &= \mathrm{A(K)} - \mathrm{A(K)}_\odot - [\mathrm{Fe/H}] - \Big(\mathrm{A}(\alpha) - \mathrm{A}(\alpha)_\odot - [\mathrm{Fe/H}]\Big) \\ &= \mathrm{A(K)} - \mathrm{A(K)}_\odot - \Big(\mathrm{A}(\alpha) - \mathrm{A}(\alpha)_\odot\Big) = \mathrm{A(K)} - \mathrm{A(K)}_\odot - [\alpha/\mathrm{H}] = [\mathrm{K}/\alpha]\end{aligned} \tag{B.2}$$

$$\begin{aligned}[\alpha/\mathrm{H}] = [\alpha/\mathrm{Fe}] + [\mathrm{Fe/H}] &= \mathrm{A}(\alpha) - \mathrm{A}(\alpha)_\odot - [\mathrm{Fe/H}] + [\mathrm{Fe/H}] \\ &= \mathrm{A}(\alpha) - \mathrm{A}(\alpha)_\odot - [\mathrm{H/H}] = [\alpha/\mathrm{H}]\end{aligned} \tag{B.3}$$

B.2 Source Function

First off, we have the definition of the source function $S_\nu \equiv \frac{j_\nu}{\alpha_\nu}$, which if expressed by Einstein coefficients become

$$S_\nu = \frac{n_u A_{ul} \psi(\nu - \nu_0)}{n_l B_{lu} \phi(\nu - \nu_0) - n_u B_{ul} \chi(\nu - \nu_0)},$$

where ψ, ϕ, χ are probability distributions describing the "natural" (due to e.g Heisenberg's principle Rutten (2003)) broadening of each Einstein coefficient. We then introduce the

Einstein relations, see equation B.4, and rewrite the source function according to equation B.5.

$$\frac{B_{lu}}{B_{ul}} = \frac{g_u}{g_l}; \qquad \frac{A_{ul}}{A_{lu}} = \frac{2h\nu^3}{c^2} \tag{B.4}$$

$$S_\nu = \frac{\frac{A_{ul}}{B_{ul}}\frac{\psi}{\phi}}{\frac{n_l}{n_u}\frac{B_{lu}}{B_{ul}} - \frac{\chi}{\phi}} = \frac{h\nu^3}{c^2}\frac{\frac{\psi}{\phi}}{\frac{g_u n_l}{g_l n_u} - \frac{\psi}{\chi}} \tag{B.5}$$

If we now assume that the probability distributions are equal, i.e $\psi = \phi = \chi$ we get the expression found in equation 2.4.

B.3 Heliocentric Correction

The orbit of the Earth relative to the Sun is in reality an ellipse, but assuming it is a perfect circle, and that the distance between the Earht and the Sun is $\sim 151 \cdot 10^9$ m. Then the orbital velocity of Earth would equal

$$v = \omega \cdot r = \frac{2\pi r}{356 \cdot 24 \cdot 60^2} \approx 30\text{km/s}.$$